



**A Method of Balancing Heat Sterilization with Minimal Media
Degradation in Microbial Astrobiology Experiments**

Submitted By

JASON KAPIT

IN PARTIAL FULFILLMENT OF THE REQUIREMENTS FOR THE DEGREE OF
MASTER OF SCIENCE IN MECHANICAL ENGINEERING

School of Engineering
Tufts University
Medford, Massachusetts

May 2009 (Corrected Version)

Signature of Author:
Jason Kapit

Certified By:
Associate Professor Douglas M. Matson
Department of Mechanical Engineering
Tufts University

Committee:
Professor Chris Rogers
Department of Mechanical
Engineering
Tufts University

Committee:
Professor Samuel Kounaves
Chemistry Department
Tufts University

ABSTRACT

Almost any imaginable experiment aimed at detecting the metabolism of astrobiological microbial life forms will require measurements to be performed on two sample systems – one that contains viable life forms, and a second, which has been sterilized to serve as a control. Successfully creating the control is essential in discerning if any signal from the non-sterile system is biogenic in nature. Accordingly, it is valuable to study how to best achieve the control condition. One of the most likely methods of creating a control is through application of heat sterilization. To effectively create a control through heat sterilization, the process must meet two requirements. First, it must inactivate viable organisms within the original sample. Second, the chemical composition of the sample after sterilization must be as similar as possible to that of the initial pre-sterilized sample. In practice, achieving these two requirements simultaneously is difficult. If a sample is heated longer and to warmer temperatures than necessary, it is likely that unwanted chemical changes will occur. On the other hand, preserving the sample's chemical properties by lowering the temperature or total process time will threaten sterilization quality.

A method of assessing the balance between sterilization quality and sample degradation was postulated consisting of generating curves called sterilization quality distributions (SQDs) for different sterilization processes. The SQD method was applied to a prototype of an astrobiology life-detection instrument that employs autoclave heat sterilization, called the Microbial Detection Array (MiDA). The final results show that a target sterilization quality can be reached up to 2.5 times faster for a dry sample than for a sample that has been mixed with water. On the other hand, stirring a sample/water mixture allows for full sterilization to be reached at a temperature that is up to 50 ° C lower than for a dry sample.

INTRODUCTION	1
THE SEARCH FOR LIFE ON MARS	1
THE MICROBIAL DETECTION ARRAY EXPERIMENT AND INSTRUMENTATION	3
STERILIZATION WITHOUT MEDIA DEGRADATION	5
BACKGROUND	8
HEAT STERILIZATION IN ASTROBIOLOGY EXPERIMENTS	8
RELATED RESEARCH WITHIN THE FOOD INDUSTRY	9
REVIEW OF MICROBIAL THERMAL INACTIVATION PRINCIPLES	11
METHODOLOGY	15
METHODOLOGY OVERVIEW	15
SAMPLE STERILIZATION QUALITY DISTRIBUTION	17
SYSTEM OF INTEREST	20
<i>The MiDA Autoclave</i>	20
<i>Sterilization Process Parameters</i>	21
<i>Relevant Samples: Organisms and Media</i>	26
THERMAL MODELING OVERVIEW	28
<i>Geometric and Material Properties</i>	30
<i>Governing Equations</i>	33
<i>Boundary Conditions</i>	35
MODELS, RESULTS, AND ANALYSIS	37
FORMULATION OF SPECIFIC SCENARIOS AND MODELS	37
MODEL VALIDATION	50
EVALUATION OF A SINGLE SCENARIO	52
TIME LIMIT SQD COMPARISON	54
TEMPERATURE LIMIT SQD COMPARISON	57
TIME-TEMPERATURE COMPARISON	59
COMPARISON BETWEEN ORGANISMS	61
COMPARISON BETWEEN SAMPLE PROPERTIES	61
CONCLUSIONS	64
ASSESSMENT OF SQD METHOD	64
RECOMMENDATIONS FOR AUTOCLAVE OPERATION UNDER VARIOUS CONSTRAINTS	64
FUTURE WORK	66
APPENDICES	67
APPENDIX A: EFFECT OF CALCULATIONS FOR THERMAL CONDUCTIVITY	67
APPENDIX B: EFFECT OF MESH SIZE	69
REFERENCES	70

Introduction

The Search for Life on Mars

Ever since the Viking Mars Landers returned ambiguous results for their life-detection experiments in the late 1970s^[3,1,4,5], there has been a heightened interest among the scientific community in studying the surface of Mars in search of past or present life. Over the past two decades, a number of additional missions in the form of both orbiters and landers have been sent to Mars. None of these missions were sent with the specific goal of searching for life, but instead, they studied the physical and chemical environment of Mars. The results from these missions have painted the surface of Mars as a harsh and desolate environment characterized by extreme cold, severe dryness, low pressure, UV bombardment, and minerals representative of acidic conditions^[6,7]. Over time, further investigation into the results of Viking's life-detection experiments also convinced the majority of the planetary science community that the reactivity of the Martian regolith found by Viking was not due to biology, but instead, to the presence of inorganic chemical oxidants that harm organic molecules^[1], a theory supported by the recent discovery of perchlorate on Mars by the Phoenix Mars Lander^[2].

Initially, these harsh environmental characteristics made it seem unlikely for life to exist anywhere on or near the surface today. However, in recent years, the discovery on Earth of a wide variety of extremophile organisms has re-ignited the search for life on Mars^[8,9,10]. Organisms have been discovered that can survive the acidity of hydrothermal vents, the cold and desiccation of Siberian permafrost, the presence of oxidizing chemicals, UV light, and even the harsh vacuum of space^[8]. Furthermore, recent findings from NASA's Phoenix Mars Lander suggest that the geochemistry at the northern latitudes of Mars exhibits several characteristics

that are conducive to life. Foremost of these discoveries is a pH similar to that of seawater on Earth when the surface regolith is wetted, and the presence of a number of inorganic nutrients, some of which organisms on Earth use as an energy source^[2]. In Mars's ancient past, and in times high obliquity, the water cycle on Mars may have allowed for liquid water to exist on the surface^[11,12]. During such times the liquid water may have mixed with soil nutrients to create conditions in which organisms could thrive. It is not inconceivable to imagine Martian life developing under such conditions and having evolved extremophile adaptations that would allow them to withstand the currently harsh environment on Mars.

Extremophiles on Earth are known to survive in completely dormant states in environments that resemble Mars for up to millions of years^[8,9], and it has been suggested that similar organisms could survive on Mars^[13,14]. It is also well known that the cold temperatures such as those found on Mars of $-80\text{ }^{\circ}\text{C}$, can act as a particularly good preservative for bacterial spores^[14]. Once warmed again, these organisms have been shown to resume their normal metabolic activities. As is common with many extremophiles living in harsh conditions on Earth, Martian organisms may currently exist in a dormant spore-like state waiting to be warmed and wetted so they can thrive once again. It is reasonable that one method of detecting such organisms would be to introduce them, along with their natural chemical nutrients, to a warm and wet environment in which they would be able to metabolize and grow. The Planetary Chemical Analysis Group in the Chemistry Department at Tufts University is currently developing a prototype of an instrument to perform such a task. It is called the Microbial Detection Array (MiDA).

The Microbial Detection Array Experiment and Instrumentation

The MiDA experiment is based upon the Wet Chemistry Laboratory (WCL) experiment that flew aboard NASA's Phoenix Mars Lander. The WCL experiment successfully acquired three samples of Martian near-surface regolith, mixed them with liquid water in separate beakers, and monitored the resulting aqueous geochemistry within each beaker using an array of chemical sensors embedded in the walls of the beaker^[15]. The MiDA experiment goes one step beyond just measuring the aqueous geochemistry within a beaker. The experiment is based on the premise that if a viable organism were present and proceeded to metabolize dissolved inorganic nutrients, such as those WCL found at the Phoenix landing site, its metabolic activity should influence the aqueous chemistry in a way that would be detectable with the sensor array. Accordingly, the MiDA instrument uses the same sensor array used by WCL, but in a new configuration that would allow for this detection of metabolic activity^[16].

Currently, a prototype of the MiDA instrument has been developed for use in proof-of-concept and field-testing experiments on Earth as shown in Figure 1. It consists of six major sub-components; 1) water chamber; 2) an autoclave sterilizer; 3) a piston with a stirrer that serves as the bottom of the autoclave; 4) a splitter; 5) a growth chamber; and 6) a control chamber. The purpose of the instrumentation is to sterilize a sample of Martian soil, mix it with water, and split it to two identical chambers, one of which serves as a control while the other is inoculated with viable microorganisms. Performing the MiDA experiment with the prototype instrument begins by collecting a fine-grained soil sample from a surface containing viable organisms, possibly extremophiles, and hand-delivering it to the autoclave sterilizer.

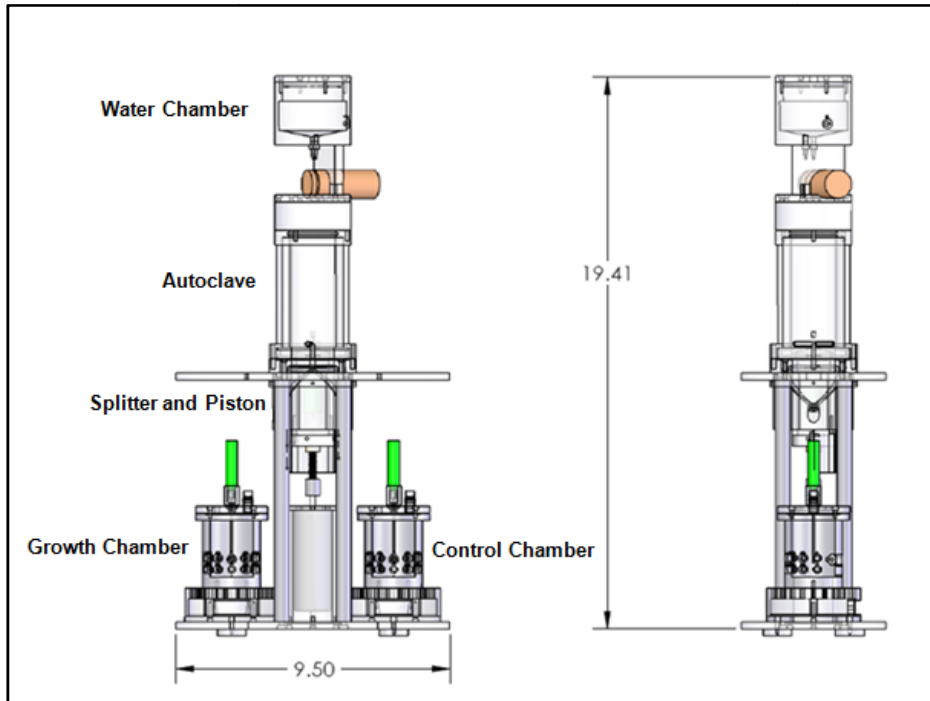


Figure 1: The Microbial Detection Array Instrument

The sterilization process is achieved by adding a variable amount of water from the water reservoir to the sample in the autoclave chamber and then using heaters on the outer walls of the autoclave to heat the sample until sterilized. The sample/water mixture is then homogenized with the stirrer. Once the piston, which serves as the bottom of the autoclave, is withdrawn from the autoclave chamber, the sample slurry is allowed to flow into the splitter where two channels evenly split it between the identical growth chamber and control chamber. The wet (and warm) chemical environments in the two chambers are then monitored by electrochemical sensor arrays similar to those used in WCL.

Initially, the sensor readings from the two chambers should be identical. Once stable readings are verified, the growth chamber is inoculated with a minimal amount of non-sterilized regolith containing viable microorganisms, and the other is left untouched to serve as a control.

One crucial characteristic of the non-sterilized sample is that it must be small enough such that no significant chemical reactions are likely upon its addition. If the microorganisms in the inoculated chamber proceed to metabolize or grow, they may cause changes in the chemical species monitored by the sensor array in the inoculated chamber in contrast to the stable signals in the control chamber. This disequilibrium in the signals would be carefully analyzed to determine if it was biogenic in nature.

Sterilization Without Media Degradation

Almost any imaginable experiment aimed at detecting astrobiological microbial life, including MiDA, requires a control to prevent a false positive result. Successfully creating a control is essential to the success of the experiment, and accordingly, it is valuable to study how such a condition is achieved. For MiDA, the control sample is created through heat sterilization within the instrument's autoclave chamber.

The success of the MiDA experiment depends on the sterilization process meeting two requirements. First, it must heat sterilize viable organisms within the original sample, and second, it must not degrade the ability of the sample to supply the nutrients needed to support the growth of viable organisms. The first requirement dictates that the time-temperature profile at any location within the sample bulk must satisfy heat sterilization requirements. The second requirement states that the chemical composition of the sample after sterilization must be as identical as possible to that of the initial pre-sterilized sample. In practice, achieving these two requirements simultaneously is not easy. If a sample is heated longer and to hotter temperatures than necessary, it is likely that unwanted chemical changes will occur. On the other hand,

preserving the sample's chemical properties by lowering the temperature or total process time will threaten sterilization quality.

For the MiDA experiment, there are two specific worries in terms of sample degradation during sterilization. The first worry is that reaching a specific temperature within the sample will activate a certain reaction, such as a melting process, the precipitation of inorganic nutrients, or the decomposition of a mineral. This means that a particular temperature may need to be avoided at all costs. The second worry is that of the degradation over time of the sample's nutrients. Many nutrients, such as amino acids and proteins, degrade with time during the sterilization process, and preserving them would argue for a sterilization process that is as short as possible. Depending on the exact degradation reactions that need to be avoided, a properly designed sterilization process can achieve a satisfactory balance between time-temperature constraints and sterilization quality.

The purpose of this master's thesis was to develop a method of assessing the balance between sterilization quality and sample preservation for a wide range of processing scenarios MiDA is capable of performing¹. Though the method developed is applicable to a wide variety of instrumentation and heat sterilization processes, the MiDA autoclave's various operational scenarios were used as a basis for forming and testing the methodology as it would apply to terrestrial organisms and earth-based tests. The investigation first involved combining concepts from microbiology and food sterilization technology to accurately predict the thermal death of microorganisms. It was then possible to integrate those principles with heat transfer models of

¹ The MiDA sterilization processing scenarios are dependent on a number of different parameters that can vary such as the sample's thermal properties, the volume of water added during the autoclaving process, and whether the MiDA stirrer is used during the autoclaving process. For a complete description of the different MiDA processes studied in this work refer to the sections called *Sterilization Process Parameters* and *Formulation of Specific Scenarios and Models*

the MiDA autoclave scenarios to generate information about process temperatures, time, and sterilization quality for each scenario. To achieve the goal of process comparison, a measurement called the sterilization quality distribution (SQD) was developed, and SQDs were generated for each process. Comparison of the SQDs for each process proved extremely useful in selecting which processes best achieved the balance between sterilization success and minimal media degradation with the MiDA autoclave chamber. The analysis performed also set a precedent in analyzing the performance of heat sterilization for use in astrobiology experiments, and it could also find use in other industries utilizing heat sterilization technology.

Background

Heat Sterilization in Astrobiology Experiments

The precedent for the use of heat sterilization (or any other type of sterilization) in an astrobiology life-detection experiment is the Viking Mission. One of the most significant results of the mission came from the Viking 1 lander's labeled release experiment, which involved adding liquid carbon-based nutrients to a Martian soil sample and monitoring the headspace above the mixture for the evolution of any carbon-containing gasses^[17]. After sample acquisition and a first round of labeled release experiments, the Viking 1 Lander heated the sample to 170 °C for three hours to sterilize it. Afterwards, the experiment was repeated to serve as a control. The results indicated that before sterilization, something in the Martian soil reacted with the carbon-based nutrients, while afterwards the sample was unreactive.

Some people believe that the difference in results before and after sterilization were due to the destruction of microorganisms that metabolized organics in the pre-sterilization experiment. They argued that these microorganisms were killed during sterilization and were rendered unviable for the post-sterilization control^[19]. However, the majority of the community believes it is quite likely that reactive chemical oxidants were initially present in the Martian soil sample and the high heat of sterilization converted them to non-reactive compounds^[1,18]. These ambiguous results highlight the concern that, while this sterilization process was probably sufficient to kill most imaginable microorganisms it may not be the most effective way to produce an experimental control. Overly-sterilizing the sample may have generated the results that were interpreted by some as the destruction of life forms.

The danger of overheating the sample for MiDA is slightly different. Sterilizing at unnecessarily high temperatures, or for longer than necessary, will not increase the likelihood of MiDA generating a false-positive result, but it could limit its ability to detect life in the first place. By heating to higher temperatures than necessary, and for longer than necessary, one may degrade the nutrient qualities of the sample such that it would not be able to support the metabolism of its native organisms. In contrast, if the sample is not heated enough, it is unlikely the experiment will generate a false-positive. Both the Labeled Release and the MiDA experiments support a point mentioned earlier; an effective sterilization process needs to kill the majority of organisms present within the sample, and it also needs to preserve the nutrient qualities of the sample.

Related Research within the Food Industry

Finding a balance between heat sterilization and the preservation of a sample's nutrients has never been studied in the context of astrobiology experiments, but investigators involved in the food technology industry have generated substantial amounts of literature on how to effectively heat sterilize organisms within canned foods before they are bought by the consumer^[20-25]. Accordingly, these researchers have developed models describing the thermal death of microorganisms within the food they study. However, those models are mostly concerned with safety issues regarding the sterilization process and not the associated risk of degrading a food's quality. A few researchers have attempted to balance the heating processes with the desire to preserve food nutrient qualities, but these analyses are limited in their scope and applicability. The studies performed have been limited to specific cases involving cylindrical cans within much larger retorts, invariable heating mediums, and heat transfer only by conduction through

steam^[26-28]. Since these studies have mostly focused on single sterilization processes, a method that successfully compares scenarios as wide ranging as those encountered with MiDA has yet to be developed.

Also, food sterilization investigators are primarily concerned with meeting sterilization safety regulations identified by parameters that are either averaged over the entire sample volume or meet a minimum sterilization criterion. For the MiDA experiment, volumetric averages of sterilization quality could be misleading when trying to optimize a process since they can't identify localized dangers, such as small areas of particularly low sterilization quality or unnecessarily high temperatures. Also, trying to satisfy a minimum criterion value may be unrealistic if a sample's chemical properties is to be preserved, since meeting such a criterion may drastically increase the process time. Furthermore, previous studies have simply never considered a maximum temperature limitation during the sterilization process, a limitation that is vital to the MiDA experiment.

The modeling methods developed for this thesis needed to improve upon previous methods of sterilization quality assessment in several ways. It needed to be applicable to a wider range of system conditions. It needed to generate localized information on sterilization quality and sample degradation, and it needed to include the ability to limit the maximum temperature during sterilization. The results also needed to lend themselves to an easy comparison between processes for their ability to achieve sterilization without sample degradation. The modeling method developed in this thesis, and the resulting QSD comparisons, meet such requirements. An introduction to the method first requires a review of microbial thermal inactivation principles.

Review of Microbial Thermal Inactivation Principles

A review of the microbiology and food technology literature, reveals that the most commonly used principle to describe the thermal death of microorganisms is the decimal reduction time (DRT).

When a concentration, C , of organisms is subjected to lethal temperature T_{ref} , the population concentration decreases with time according to first-order kinetics^[20]:

$$\text{at } T_{ref}: \quad -\frac{dC}{dt} = k_{ref}C \quad \text{EQ. 1}$$

If EQ. 1 is integrated and an initial concentration of C_0 is assumed, the result is an exponential decay equation that describes the reduction of a population of microorganisms with time:

$$C(t) = C_0 e^{-k_{ref} \cdot t} \quad \text{EQ. 2}$$

where the magnitude of k_{ref} describes the rate at which the concentration decreases with time at temperature T_{ref} . The decimal reduction time, $D_{T_{ref}}$, of an organism at T_{ref} is the length of time required for the organism concentration to decrease by a factor of 10, and accordingly it is defined as:

$$D_{T_{ref}} = \ln(10) / k_{ref} \quad \text{EQ. 3}$$

When EQ. 3 is combined with EQ. 2, the result is equivalent to:

$$C(t) = C_0 \cdot 10^{-t/D_{T_{ref}}} \quad \text{EQ. 4}$$

To illustrate EQ. 4, if organisms are subjected to constant temperature T_{ref} for a time of $D_{T_{ref}}$, they will decrease in concentration by one order of magnitude. Similarly, if they are subjected to T_{ref} for a time of $5D_{T_{ref}}$, they will decrease in concentration by five orders of magnitude. These

quantifications of sterilization are called F_p values, and they characterize the quality of a sterilization process. F_p is formally defined as:

$$F_p = D_{T_{ref}} \cdot (\log C_1 - \log C_2) \quad \text{EQ. 5}$$

where C_1 and C_2 designate the change in concentration. The decimal reduction time at a reference temperature is a useful concept, but it is inadequate to characterize the thermal death of organisms that are subject to real thermal processes. At minimum, most sterilization procedures require a period of heating followed by a cooling phase. Accordingly, the temperature is not constant over time, and it is necessary to describe how the decimal reduction time, D_T varies with temperature:

$$\text{at } T: \quad D_T = D_{T_{ref}} \cdot 10^{(T-T_{ref})/z} \quad \text{EQ. 6}$$

and at an arbitrary temperature:

$$C(t) = C_0 \cdot 10^{-t/D_T} \quad \text{EQ. 7}$$

EQ. 6 introduces the z -value which is the change in temperature that causes the decimal reduction time to change by a factor of 10. Values for $D_{T_{ref}}$ of organisms are determined empirically, and the z -value is determined by empirically measuring how D_T varies between different temperatures. EQ. 6 can be linked to EQ. 5 to describe the sterilization quality F_p of an arbitrary process. This is done by inserting EQ. 6 into EQ. 7, taking the logarithm of both sides, differentiating with respect to time, and remembering that temperature is a function of time. The result is:

$$\text{For } T(t): \quad \frac{d(\log C)}{dt} = \frac{1}{D_{T_{ref}}} \cdot 10^{(T(t)-T_{ref})/z} \quad \text{EQ. 8}$$

Integrating EQ. 8 gives:

$$\int_{C_1}^{C_2} d(\log C) = \frac{1}{D_{T_{ref}}} \cdot \int_{t_1}^{t_2} 10^{(T(t)-T_{ref})/z} dt \quad \text{EQ. 9}$$

and

$$D_{T_{ref}} \cdot (\log C_1 - \log C_2) = \int_{t_1}^{t_2} 10^{(T(t)-T_{ref})/z} dt \quad \text{EQ. 10}$$

substitution of EQ. 5 yields:

$$F_p = \int_{t_1}^{t_2} 10^{(T(t)-T_{ref})/z} dt \quad \text{EQ. 11}$$

EQ. 11 is the key to characterizing a full thermal process because it allows for a quantitative indicator that describes the quality of sterilization for an arbitrary process, F_p , which can be compared to the F value of a sterilization process that is known to achieve a certain result, such as one at a constant lethal temperature.

The quality of sterilization, characterized by F_p is particularly valuable when trying to minimize the impact the sterilization process has on the chemical properties of a sample. The formulation implies that there are several different time-temperature profiles that can result in the same quality of sterilization. For instance, one may want to avoid the temperature at which a mineral would decompose. In such a case, it may be worthwhile to run a process at a lower maximum temperature for a longer time. Alternatively, a thermal degradation reaction, such as

that of an amino acid, may occur according to first order kinetics. In that case, it might make sense to ramp the temperature to a high value very quickly, allowing for a shorter process and lessening the length of time when the degradation is occurring.

The above equations also imply that there is no well defined criterion for defining what constitutes a “sterile” condition, and what should be measured over the sterilization process is the probability of survival. The probability of survival decreases exponentially with time, so it never reaches zero. For example if a population of 10^8 organisms is subjected to a $F = 10D$ process, then the probability of survival of a single organism at the end of the process is 1 in 100. In order to properly assess and compare different MiDA sterilization process, it is necessary to predict probabilities of survival throughout the sample. Since F values vary significantly throughout the sample, it was useful to define a new dimensionless measure of sterilization quality, Q , which is the logarithm of the F_p value divided by a target F value:

$$Q = \log \left(\frac{F_p}{F_{Target}} \right) \quad \text{EQ. 12}$$

F_{Target} is defined from a desired decimal reduction using EQ. 5. Accordingly, a Q value at or above 0 indicates that the target sterilization level has been reached. The following section describes how the SQD method was used to assess the sterilization quality (Q) throughout the sample at any point in time for different sterilization processes.

Methodology

Methodology Overview

The methodology section describes the steps taken for generating the sterilization quality distributions (SQDs) that served as a basis of comparison for different MiDA sterilization processes. A detailed description of the steps is given in the subsequent methodology subsections, but a brief overview of the steps and an example of an SQD is given below.

1. First, a system of interest was identified for study. This involved defining the sterilization instrumentation and identifying process parameters that may affect the temperature profile seen by the sample. For this work, the system was the MiDA autoclave, and examples of variable process parameters included the sample volume, sample location, water content, and the stirrer state. Identifying a the system of interest also included selecting appropriate microorganisms and media.

For this work, the sample consisted of either *Escherichia coli* or *Bacillus subtilis* living on a fine-grained quartz-sand medium.

2. Second, a thermal model was generated for each MiDA sterilization scenario. This involved defining parameters relating to the physical and thermal properties of the instrumentation. Next, governing differential equations and appropriate boundary conditions were identified. The heat transfer models for each scenario were solved numerically with Comsol Multiphysics FEA software to yield a transient temperature profile throughout discrete regions of the sample bulk.

3. Third, the transient temperature profile within the sample was related to the sterilization of microorganisms. This was done by meshing the sample region, and assuming that a certain concentration of viable organisms was represented at each point in the mesh. By selecting a specific organism, such as E coli or bacillus subtilis, the thermal death of the organism concentration at each mesh point was modeled using EQ. 11 and inserting the temperature of the mesh point for $T(t)$. In the case for which an organism had the possibility of moving with fluid, such as that involved with natural convection in a sample-water system, the velocity profile was combined with the temperature profile to determine $T(t)$ for the moving organisms.

4. The final result was a quantification of sterilization quality with time $Q(t)$ throughout the sample. A SQD could be generated at any point in time by plotting a probability distribution of sterilization values throughout the entire sample region. This allowed for the SQDs for any number of processes to be compared at any point in time.

In order to better understand the methodology described above, and for it to be further developed in the upcoming sections, is useful to first consider a sample SQD. The example below will clarify the methodology by giving a concrete sample of its final goal and application.

Sample Sterilization Quality Distribution

An example of two hypothetical SQDs is shown in Figure 2, and a comparison between them illustrates the usefulness of SQDs when assessing and comparing heat sterilization processes.

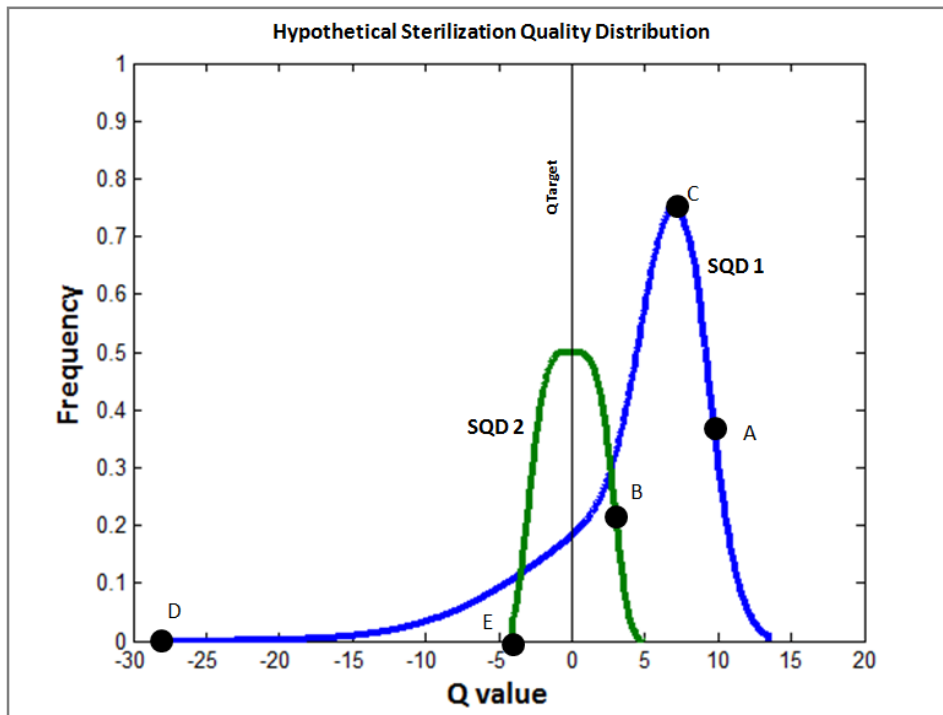


Figure 2: Sample SQDs

SQD 1 and SQD 2 represent two hypothetical sterilization processes 1 and 2, and it will be assumed that they are plotted at exactly the same time during each process (which may not always be the case), say at $t = 5$ min. To reiterate, these two curves would be generated using the steps described in the *Methodology Overview* section, and the method will be elaborated upon in later sections. If it is assumed that an initial concentration of organisms is distributed evenly throughout a discrete number of points within the sample bulk, Q values throughout time can be

calculated at each of those points. In Figure 2, each point on the two curves represents a number of points in the sample in each process that have experienced a cumulative time-temperature profile resulting in a certain Q value at $t = 5$ min. Higher Q values, such as that designated by point A, indicate regions of the sample that have experienced higher cumulative time-temperature effects than points further to the left, such as points B, C and D. Higher frequency values are indicative of larger portions of the sample having similar cumulative time-temperature history and thus, a similar Q value. For example, point C on SQD 1 signifies that a high portion of the sample has a Q value of approximately 7 at $t = 5$ min, whereas a large portion of the process 2 sample has a Q value of 0 at $t = 5$ min. In general, high frequency values can signify regions large regions over which the temperature profile has been similar, or it can signify separate regions that have experienced similar temperature histories, possibly due to symmetries. In either case, the location of peaks in the SQD are often indicative of the overall sterilization quality at any particular point in time.

When assessing SQDs, it is often useful consider the relationship of the curve with respect to the full sterilization value of $Q = 0$. This relationship in Figure 2 highlights the danger of using volumetric averaging or a minimum Q criterion to determine when a certain level of sterilization has been reached. For both processes, an averaged sterilization quality value would indicate that the sample has reached full sterilization, even though significant portions of both samples are still below F_{Target} . The SQD makes it clear that this is actually not the case. The danger of assigning a minimum Q value for an arbitrary process is illustrated as well. For example, it may take unrealistic length of time for the SQD of process 1 to fully pass $Q = 0$, thus degrading the sample quality or unnecessarily draining time and power. The SQDs avoid these dangers by displaying sterilization information throughout the entire sample distribution. They

reveal that it may be more worthwhile to run process 1 for slightly longer (moving the SQD to the right) until a reasonable total level of sterilization is reached, or to simply choose process 2.

The SQDs also lend themselves to an easy comparison between the two processes at time $t = 5$ min. The relation of the SQDs to $Q = 0$ gives important information in making decisions that can help balance sterilization quality with total time and temperature effects and thus preserving the sample's chemical properties. For example, a much larger portion of process 1 is fully sterilized than for process 2, and if a time of 5 minutes is a limiting factor in the sterilization process, process 2 should be chosen over process 1. On the other hand, if the processes can be run for slightly longer, it is likely that process 2 will fully pass the target sterilization criterion much faster than process 1, since point E will pass $Q = 0$ long before point D. Such information is extremely valuable when selecting between sterilization processes.

It is left to the results and analysis section to show that through varying the criterion for the point in time when the SQDs are compared, one can gain more significant information for use in comparing the balance between time, temperature and sterilization quality for a variety of different processes. The rest of the methodology section describes in detail how SQDs were generated for a number of different MiDA sterilization processes, and as described in the previous section, the first step was to define the system of interest.

System of Interest

The MiDA Autoclave

The system of interest was the MiDA autoclave, for which a CAD drawing is shown in Figure 3.

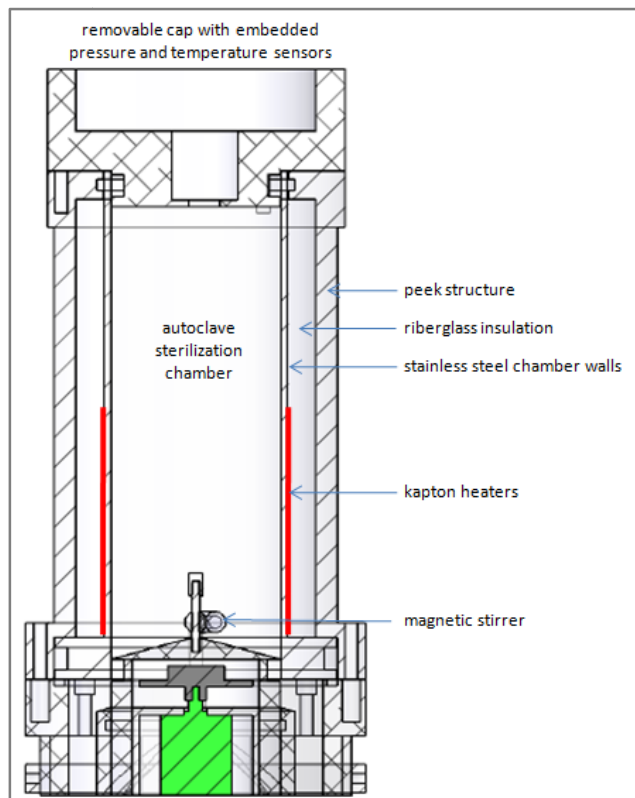


Figure 3: MiDA Autoclave Structure

The autoclave chamber is a hollow cylinder with inner walls made from stainless steel. The other structural materials consist of shells of varying thickness made from fiberglass insulation, and PEEK. The cap on top is made of PEEK and contains sensors for monitoring the pressure and temperature within the autoclave. The piston on the bottom is made of PEEK as well, and it houses a magnetic stirrer that can be used to mix a sample slurry during the sterilization process. The stir bar is made of Teflon and its presence will be neglected in all

calculations due to its small size relative to the sample volume. A sample of fine particles with viable organisms is introduced to the chamber by removing the cap, placing the sample within the chamber, and then replacing the cap. Before beginning the sterilization process, the MiDA instrumentation has the ability to add up to 100 mL of water from the water reservoir to the autoclave chamber. The sterilization process is initiated by turning on the kapton heaters and leaving them on for a prescribed amount of time or until a specified temperature profile is matched. Based on the capabilities of the instrument, and depending on the requirements of a specific MiDA experiment, it is possible to implement a wide range of different sterilization scenarios. These scenarios are elaborated upon in the following section.

Sterilization Process Parameters

Depending on the requirements of any particular MiDA experiment, several factors, or process parameters, can be adjusted that will alter the sterilization process. A proper characterization of the MiDA autoclave required modeling several scenarios that were representative of possible changes in those process parameters. The goal of defining these scenarios was two-fold. First, they needed to result in vastly different thermal profiles within the sample bulk to prove that the SQD method was applicable to widely varying scenarios. Second, they needed to cover the extent of MiDA's capabilities to aid in the decision-making processes during MiDA operation. The possible scenarios characterized in this work were defined by adjusting the following process parameters:

1. the total sample volume
2. the sample material

3. the distribution of the sample within the autoclave chamber
4. the choice of microorganism

and if water is added:

5. the volume of water mixed with the sample for the sterilization process
6. adhesion of the organisms to the sample bulk
7. the use of the autoclave stirrer

By varying each of the above parameters, it was possible to formulate a variety of different scenarios and a corresponding thermal model for each scenario. QSDs can be generated from those models to serve as a basis for assessing the balance between sterilization and minimal media degradation for each scenario. Each of the characteristic parameters were chosen since it was expected that varying them would have significant influence on the rate of heat transfer, and accordingly the temperature, within the sample bulk. Some system parameters like the location or the heat flux from the heaters was cannot be varied. To clarify each of the characteristic parameters listed above, it is worthwhile to define and briefly discuss each one individually.

1. Total Sample Volume

The total sample volume is simply the entire volume of sample bulk placed into the autoclave chamber, regardless of where it is located and before it is mixed with any water.

2. *Sample Material*

It was expected that the *sample material* would have a significant influence on the thermal properties of the sample bulk, which are related to the sample material's thermal conductivity, k (W/m·K), specific heat, C_p (J/kg·K), and density, ρ (kg/m³). It should be noted that these properties correspond to the sample's individual particles and not the sample bulk. The thermal properties of the sample bulk are characterized by a combination of the sample's thermal properties and the thermal properties of the fluid that occupies the gaps between sample particles, which is usually air or water (described in the section called *Geometric and Material Properties*).

3. *Sample Distribution*

The sample distribution is more of a qualitative measure and can be described as the geometry of the sample within the autoclave chamber. For example, the sample bulk would nominally be located at the bottom of the chamber distributed such that it is in contact with both the bottom and side walls of the chamber. This case is referred to as a "wide" distribution. However, a case may occur such that the sample bulk ends up on the bottom of the chamber but does not contact the inner walls. This scenario is referred to as a "narrow" distribution.

4. *The Choice of the Microorganism*

The choice of the microorganism primarily influences its thermal sterilization characteristics. The sterilization characteristics of the organisms are defined by the organism's decimal reduction time, $D_{T_{ref}}$, T_{ref} , and its z-value as described in Table 1.

5. Volume of Water Added

The volume of water mixed with a sample is defined as a volume, in mL, of deionized water that is added to the sample before the sterilization process begins. There are two characteristic amounts of water that will be considered. First, the total water volume added is just enough to simply fill the porous gaps between sample particles. This amount of water will be called a “minimal” amount of water. The second characteristic amount occurs when the total amount of water added equals the minimal matrix amount plus a volume of water that is equal to or greater than the total sample volume. This will be called an excess amount of water.

6. Adhesion of the Microorganisms to the Sample Bulk

The adhesion of the microorganisms to the sample bulk was taken into consideration only when there was excess level of water in solution and the stirrer is off, giving particles and organisms space to move within the natural convection in the fluid above the sample. Admittedly, it is almost impossible to predict if and how the microorganisms would enter and move throughout the naturally convecting water above the sample. However, it is arguable that many Earth organisms have a density similar to water, and it is hypothetically possible to consider the case in which such organisms would enter the liquid water phase above the sample and follow the flow of the water. Two extreme cases of organism adhesion to the sample bulk will be considered in this work. Either they will remain immobilized within the sample bulk, or a certain initial concentration will begin uniformly distributed within the liquid above the sample, and will exactly follow the naturally convecting flow that develops during the heating process.

7. *Stirrer Operation*

In the case when there is excess water, the autoclave contains a stirrer which can be used to stir a sample/water mixture. When the stirrer is off, only a small portion of the sample/organisms can enter the fluid water phase above the sample. When the stirrer is on, it is assumed that the entire sample/water mixture is fluidized such that the particle density and temperature profile within the mixture are both uniform.

It is also relevant to discuss a few other parameters that will intentionally not be varied. The first of these parameters is the sample grain size and shape. For simplicity, it will be assumed that the sample's particles are all spherical in shape and uniform in size at less than 1mm in diameter. Accordingly the grain size and shape of the individual particles do not influence the heat transfer throughout the sample bulk, and it only the sample particle to sample matrix volumetric ratio that influences the sample bulk's thermal properties. It will be assumed that this ratio is $0.64^{[34]}$, which is commonly used to describe the ratio that occurs when a sample is poured into a pile.

Second, the size, and thermal properties of the microorganisms will be ignored. It will be assumed that the organisms are small enough such that their temperature is exactly coupled with their surrounding environment. It will also be assumed that there are no significantly large clumps of microorganisms located anywhere in the sample, so that their size and thermal properties do not affect the heat transfer through the sample bulk or to the location of any of the organisms.

From the six process parameters discussed above, seven representative scenarios were generated (see *Formulation of Specific Models and Scenarios*), and it was then necessary to select specific organisms and media to insert into those scenarios.

Relevant Samples: Organisms and Media

The specific choice of organisms and sample properties to serve as a basis for analysis are those that are relevant to the MiDA experiment. Although MiDA is an astrobiology instrument designed to eventually detect life on Mars, it is still in a proof-of-concept phase that involves performing tests on Earth, and while it is interesting to speculate about the possible properties of astrobiological life, there is too much uncertainty to provide the basis for theoretical analyses involving such organisms. Accordingly, for method development, it will be assumed that the instrument is being used on Earth and that the organisms are bacteria relevant to Earth tests. Once a variety of proof-of-concept tests have been performed for Earth organisms, it would be left up to the instrument investigator to apply what has been learned to the case of other speculative forms of life.

It is reasonable to start with two organisms that can easily be used for Earth testing. The first one, *Escherichia coli*, was chosen since it is representative of a wide variety of Earth microorganisms. It is very easy to obtain and testing with *E coli* is generally quite simple. The second, the extremophile *Bacillus subtilis*, was chosen since it is generally considered the most likely Earth candidate to represent the characteristics of an organism that would survive on Mars. The fact that there is a large amount of literature on both organisms also makes them suitable choices. To describe the thermal death of both *E coli* and *Bacillus subtilis*, values for T_{ref} and z

for both E coli and for bacillus subtilis were retrieved from the literature and are summarized in Table 1. Literature also provided typical ingredients that a sample must contain in order to support the growth of both organisms, and they include various combinations of the nutrients in

Table 2. Since it is also unknown what exact media organisms will be growing on during Earth testing, it was assumed that the sample would be comprised one of Earth's most common minerals, quartz sand, and it was assumed that the sandy sample would contain the nutrients in

Table 2.

Table 1: E coli and Bacillus subtilis sterilization characteristics

Organism	T_{ref} (°C)	D_{Tref} (min)	z (°C)
<i>Escherichia coli</i>	58	2.5	4.8
<i>Bacillus subtilis</i>	100	11	7

Table 2: Sample nutrients

Typical Nutrients
K ⁺ , PO ₄ ³⁻ , Na ⁺ , SO ₄ ²⁻ , NO ₃ ⁻ , NH ₄ ⁺ , Fe ²⁺ , Ca ²⁺ , Mg ²⁺ Cl ⁻ , acetate, along with various amino acids, carbohydrates, or proteins. ²

² To justify earlier claims about the need to achieve a balance between sterilization and media degradation, Table 1 and Table 2 illustrate the need for such a balance. First off, the sterilization process must effectively reduce the number of organisms within the sample to an acceptable level, and that process is characterized by the parameters in Table 1. Second, heating various combinations of the nutrients in Table 2, may cause unwanted chemical reactions. For instance, the denaturing of amino acids and proteins in the range of 90-120 C is of particular concern^[37]. Also, at high temperatures, a system involving varying concentrations of the nutrients in Table 2 may precipitate phosphate below 120 C and may release NH₃ gas into the headspace at temperatures as low as 55 ° C^[36]. If these maximum temperature reactions are of concern, it would suggest that the entire sterilization process should proceed at as low of a temperature as possible to ensure minimal sample degradation.

A time degradation may also be of concern. For example, amino acids degrade according to first order kinetics just as organisms do, and it is convenient, and perhaps lucky, that their degradation rate is often much slower than the death rate of most organisms at a specific temperature. Such a relationship suggests that to both maximize sterilization and nutrient preservation, the sterilization process should proceed as quickly as possible. Regardless of the degradation concern, the SQDs generated will be useful in comparing processes to avoid such unwanted thermal reactions.

Thermal Modeling Overview

For the third step in creating SQDs for comparison of MiDA scenarios, appropriate thermal models were formulated and solved. It is of course impossible to predict and model every possible scenario that includes different combinations, levels, and types of influence from characteristic parameters 1-7. Therefore, seven representative scenarios were formulated to be wide-ranging enough to characterize MiDA's operation and demonstrate the applicability of the SQD method to a set of significantly different thermal processes. These scenarios were categorized under two cases distinguished by whether or not water is present during the sterilization process. A third case, was also included to serve as a validation of the thermal modeling procedures. Before each of the cases and models are described in detail, it is useful to identify terminology, governing equations, the boundary conditions used in defining and describing each thermal model.

For the upcoming discussion of each thermal model, the terms subdomain and boundary will be used frequently as shown in Figure 4. A subdomain is a region of the model that is characterized by a set of well-defined material properties, that has a well-defined geometric border, and whose behavior is governed by set of specified differential equations. For example, the stainless steel inner cylinder, the fiberglass insulation, the air within the autoclave, and the sample bulk are all considered separate subdomains. Boundaries are defined as the interface at which two subdomains come into contact. For example, the interface between the air and the stainless steel inner cylinder and the interface between the air and the sample bulk, are boundaries.

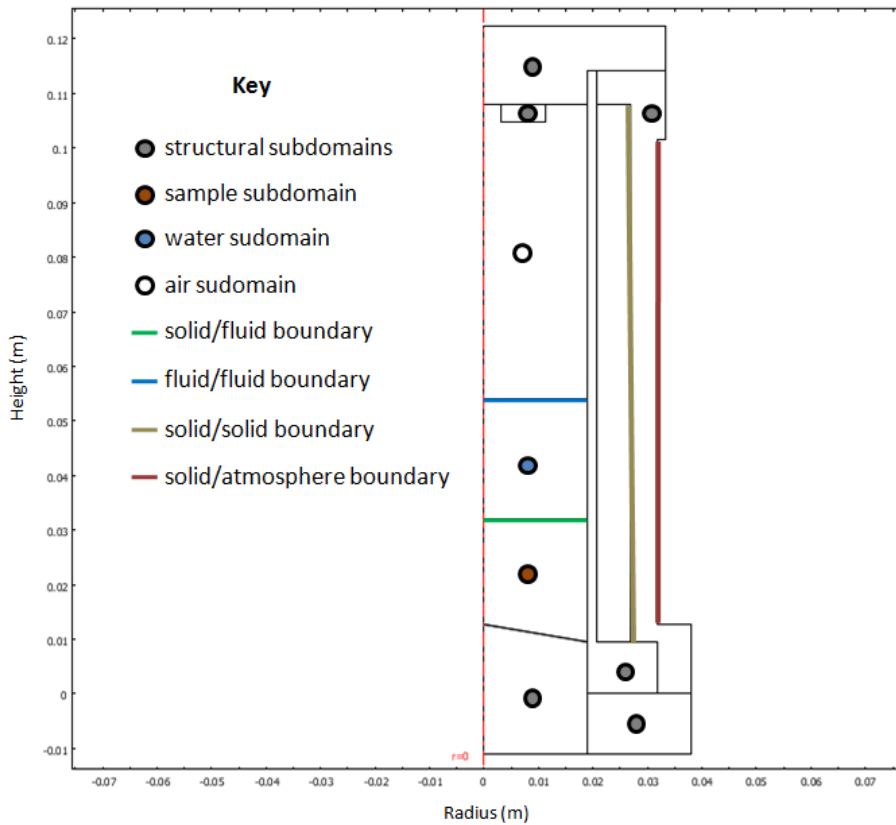


Figure 4: MiDA geometry subdomains and boundaries (dimensions in meters)

Accurately defining each model involved several steps. First, the geometry of the model was accurately specified. Second, each subdomain was assigned a set of governing differential equations describing heat transfer and, if necessary, fluid flow. Third, material properties for each subdomain were identified. Lastly, boundary conditions were assigned to allow for the solution of the subdomain's differential equations. By making adjustments during each of the four previous steps, it was possible to create the seven representative thermal model scenarios. The process of defining the geometry, governing equations, material properties, and boundary settings for a number of models are described in the following sections.

Geometric and Material Properties

To begin the modeling process, CAD diagrams of the MiDA autoclave were translated into COMSOL in order to define the basic geometry for the autoclave thermal models. The overall dimensions of the autoclave components can be seen in Figure 4 where the units are in meters. Sample subdomains, and if necessary, liquid water subdomains were added to the geometry. Since the geometry of those subdomains was affected by characteristic parameters such as sample volume, sample distribution, and water volume, they were adjusted appropriately when those parameters were varied.

Next, thermal and fluid material properties were identified for each subdomain of the model, and those properties are listed in Table 3.

Table 3: Material Properties and Equations

Material	k (W/m·K)	ρ (kg/m ³)	C_p (J/kg·K)	η (Pa·s)
PEEK	0.25	1310	320	N/A
Stainless Steel	16.2	8030	500	N/A
Fiberglass Insulation	0.03	140	844	N/A
Air	$10^{0.8616 \cdot \log_{10}(\text{abs}(T)) - 3.7142}$	$p \cdot \frac{0.0288}{8.314T}$	$0.0769 \cdot T + 1076.9$	$-7.887E - 12 \cdot T^2 + 4.427E - 08 \cdot T + 5.204E - 06$
Water	$0.0015 \cdot T + 0.1689$	lookup table	4200	lookup table
Quartz Sand	3	2620	830	N/A
Sample Bulk	EQ. 15	EQ. 16	EQ. 16	N/A

*All mineral thermal conductivity parameters determined from [35]. All mineral C_p and ρ data from [38].

In order to properly describe the thermal conductivity within the sample bulk, it was necessary to review literature^[30] on the thermal conductivity of packed particle beds, where the particles have thermal conductivity, K_s , and the matrix (of gas or liquid) has thermal conductivity,

K_f . This review suggested that simple volumetric averaging becomes increasingly inaccurate as to $K_s/K_f > 10$. It also showed that limits for the effective thermal conductivity of such a system, k_{eff} , are described by Maxwell's lower and upper bounds:

$$\begin{array}{l} \text{Maxwell Lower} \\ \text{Bound:} \end{array} \quad \frac{k_{eff}}{k_f} = \frac{2\varepsilon + (3 - 2\varepsilon)k_s/k_f}{3 - \varepsilon + k_s/k_f} \quad \text{EQ. 13}$$

$$\begin{array}{l} \text{Maxwell Upper} \\ \text{Bound:} \end{array} \quad \frac{k_{eff}}{k_f} = \frac{2(k_s/k_f)^2(1 - \varepsilon) + (1 + 2\varepsilon)k_s/k_f}{\frac{(2 + \varepsilon)k_s}{k_f} + (1 - \varepsilon)} \quad \text{EQ. 14}$$

where ε is the volumetric ratio of particles to matrix, assumed to be 0.65. However, for cases where $K_s/K_f > 100$, such as for quartz particles in a matrix of air, the predictions of these bounds can be off by up to an order of magnitude, thus significantly affecting the final SQDs³. Intermediate ground between the upper and lower bounds was found by using a formulation called, Hadley's weighted average, which is a combination of Maxwell's upper bound and a weighted average expression. According to experimental data, this equation most accurately describes the effective thermal conductivity of packed particle beds for a wide range of K_s/K_f values:

³ To determine the effect of the equation selected to predict k_{eff} , three thermal models were generated for scenario 1A (see section called *Formulation of Specific Scenarios and Models*) using each of the three predictions. The resulting SQDs showed significant variations in the length of time to reach full sterilization. The Hadley weighted average was chosen as an intermediate between the extremes and for its agreement with experimental data.

$$\begin{array}{l}
\text{Hadley} \\
\text{Weighted} \\
\text{Average:}
\end{array}
\quad
\frac{k_{eff}}{k_f} = (1 - \alpha_0) \frac{\varepsilon f_0 + k_s/k_f(1 - \varepsilon f_0)}{1 - \varepsilon(1 - f_0) + f k_s/k_f \varepsilon(1 - f_0)} + \alpha_0
\quad \text{EQ. 15}$$

· (Maxwell Upper Bnd)

Where $\alpha_0 = -1.084 - 6.778(\varepsilon - 0.289)$, and $f_0 = 0.8 + 0.1\varepsilon$. The Hadley weighted average was used for all predictions of k_{eff} in the sample subdomain.

For the simpler cases of specific heat, and density, a simple volumetric average was appropriate for calculating calculate C_p and ρ within the sample bulk:

$$\begin{array}{l}
\text{Volumetric} \\
\text{average:}
\end{array}
\quad
p_{eff} = (1 - \varepsilon)p_s + \varepsilon p_f
\quad \text{EQ. 16}$$

where p_s , p_f and p_{eff} are the C_p or ρ for the sample particles, the matrix, and the sample bulk respectively.

This is an appropriate point to mention that, when water was present in the autoclave during the sterilization process, the water vapor content in the gas phase above the sample was neglected in all cases. In reality water vapor pressure would increase due to heating and be driven into the air above the sample, but the majority of that air would then condense on the upper cooler walls of the autoclave. Therefore, minimal water vapor content would be in the gas phase at any particular time. Therefore, for this thesis it was sufficient to neglect the effect of water vapor, and simply consider only air in the headspace.

Governing Equations

For proper thermal analyses, all of the models need to include both conductive and convective heat transfer. Certain subdomains required an analysis dominated by conduction, and others required both conduction and convection to be modeled. To properly describe the convective and conductive heat transfer within the autoclave, it was necessary to identify the appropriate differential equations^[40] governing these phenomena. Application of these equations to the various autoclave thermal models is described in *Formulation of Specific Scenarios and Models* section.

For subdomains in the autoclave that are dominated by conduction, there is no internal volumetric heat generation, and the transient nature of the temperature profile is required. Accordingly it is proper to apply the diffusion equation to describe conservation of energy in areas in the autoclave where conduction dominates:

$$\begin{array}{l} \text{conduction energy} \\ \text{conservation:} \end{array} \quad \rho C_p \frac{\partial T}{\partial t} - \nabla \cdot (k \nabla T) = Q \quad \text{EQ. 17}$$

where ρ is the material's density, C_p is the material's heat capacity, T is temperature, k is the material's thermal conductivity, Q is the total heat flux, and t is time.

Subdomains in which heat transfer is dominated by conduction include the structural elements of the autoclave and the sample bulk. Admittedly, small regions of natural convective flow could may arise in the liquid or air matrix within the sample bulk, but as long as the particle size is less than 1 cm in diameter, these heat transfer effects are negligible^[30].

In subdomains where conduction and convection are both influential, it was necessary to describe the transfer of energy, as well as the transfer of mass and momentum. For modeling purposes, liquids were described with the Navier-Stokes equations simplified for incompressible fluids, and gasses were described with the Navier-Stokes equations simplified for weakly compressible fluids. Such assumptions are reasonable since the compressibility of fluids is very small at the temperatures within the autoclave, whereas gases will see significant density variations when subjected the same temperatures.

For both the incompressible and weakly compressible cases, the energy balance is the same:

$$\begin{array}{l} \text{convection energy} \\ \text{conservation:} \end{array} \quad \rho C_p \frac{\partial T}{\partial t} + \nabla \cdot (-k \nabla T) = Q - \rho C_p \mathbf{u} \cdot \nabla T \quad \mathbf{EQ. 18}$$

where \mathbf{u} is the velocity vector of the fluid.

For the incompressible case, the general Navier-Stokes mass and momentum conservation equations simplify to:

$$\begin{array}{l} \text{mass} \\ \text{conservation:} \end{array} \quad \nabla \cdot \mathbf{u} = 0 \quad \mathbf{EQ. 19}$$

$$\begin{array}{l} \text{momentum} \\ \text{conservation:} \end{array} \quad \rho \frac{\partial \mathbf{u}}{\partial t} + \rho \mathbf{u} \cdot \nabla \mathbf{u} = \nabla \cdot [-p \mathbf{I} + \eta (\nabla \mathbf{u} + (\nabla \mathbf{u})^T)] + \mathbf{F} \quad \mathbf{EQ. 20}$$

where p is the pressure, \mathbf{F} is the buoyancy force, η is the viscosity, and \mathbf{I} is the identity matrix.

and for the weakly-compressible case, the general Navier-Stokes equations simplify to

$$\begin{array}{l} \text{mass} \\ \text{conservation:} \end{array} \quad \frac{\partial \rho}{\partial t} + \nabla \cdot (\rho \mathbf{u}) = 0 \quad \mathbf{EQ. 21}$$

$$\text{momentum conservation: } \rho \frac{\partial \mathbf{u}}{\partial t} + \rho \mathbf{u} \cdot \nabla \mathbf{u} = \nabla \cdot \left[-p\mathbf{I} + \eta(\nabla \mathbf{u} + (\nabla \mathbf{u})^T) - \left(\frac{2\eta}{3} - \kappa_{dv} \right) (\nabla \cdot \mathbf{u})\mathbf{I} \right] + \mathbf{F} \quad \text{EQ. 22}$$

Boundary Conditions

In order to solve the above sets of differential equations, a proper assignment of boundary conditions between subdomains (Figure 4) was required. At interfaces only involving conduction, only thermal boundary conditions need to be provided, but at interfaces involving convection, both thermal and fluid flow boundary conditions were necessary. There were a limited number of heat transfer and fluid flow boundary types that arose when creating the seven representative models, and they are outlined in the tables below^[40].

Heat Transfer Boundary Conditions

Interface	Boundary Equation	Description	Name
solid/solid	$\mathbf{n} \cdot (k_1 \nabla T_1 - k_2 \nabla T_2) = 0$	Heat flux continuous across boundary	BC 1
solid/fluid	$T_1 = T_2$	Temperature continuous across boundary	BC 2
fluid/fluid	$\mathbf{n} \cdot (\mathbf{q}_1 - \mathbf{q}_2) = 0$ $\mathbf{q}_i = -k_i \nabla T_i + \rho_i c_{pi} T_i \mathbf{u}_i$	Heat flux continuous across boundary	BC 3
solid/atmosphere	$\mathbf{n} \cdot \mathbf{q} = h(T - T_{amb})$	convective heat flux, h defined from [39]	BC 4
solid/heater/solid	$\mathbf{n} \cdot (k_1 \nabla T_1 - k_2 \nabla T_2) = q$	Heat flux across boundary changes by q. Heaters extend 2" up the wall and q = 5800 W/m ²	BC 5

Fluid Flow Boundary Conditions

Interface	Boundary Equation	Description	Name
fluid/solid	$\mathbf{u} = \mathbf{0}$	no slip; fluid velocity is zero	BC 6
liquid/gas (for liquid phase)	$\mathbf{n} \cdot \mathbf{u} = 0$ $\mathbf{u} \cdot \mathbf{t} = U_w$ $\mathbf{t} = (-n_z, n_r)$	Sliding wall; fluid velocity is tangent to the wall at a prescribed velocity U_w	BC 7
gas/liquid (for gas phase)	$\mathbf{n} \cdot \mathbf{u} = 0$ $\mathbf{t} \cdot [-p\mathbf{I} + \eta(\nabla\mathbf{u} + (\nabla\mathbf{u})^T)]\mathbf{n} = 0$	Wall slip; no normal velocity, tangential velocity is unimpeded	BC 8

It noteworthy to mention assumptions being made for two of the above boundary conditions. For the liquid/gas and gas/liquid interface, it is assumed that momentum effects from the gas flow are negligible compared to the effect of the fluid momentum. Thus, the velocity at the boundary is dominated by the fluid. This is commonly the case for liquid and gas interfaces^[31]. Accordingly, at the boundary the flow of the fluid is modeled by a full slip condition (no impedance from the gas) and the flow of the gas at the interface is set to equal that of the unimpeded fluid.

Models, Results, and Analysis

Formulation of Specific Scenarios and Models

The seven scenarios for which thermal models and SQDs were generated are now described in detail. To organize the models, they are grouped into three cases. The description of each model scenario includes a discussion of the appropriate geometry, governing equations, boundary conditions, and locations of the organisms. Each of the models described below was solved numerically in Comsol Multiphysics for a transient 2D axially symmetric case using Lagrange quadratic elements. Transient temperature profiles and flow fields were obtained from the models out to a time of 2500 seconds.

Case 0: Thermal Model Validation

This case was not considered part of the representative models designed to demonstrate the SQD method or characterize a real MiDA sterilization process. Instead, it was a model used to validate the modeling process against experimental data.

Model 0A

Model 0 was simply the case in which dry air is the only substance in the autoclave and the stirrer is off when the sterilization process is run Figure 5. Once the autoclave heaters are turned on, heat is transferred through the stainless steel walls of the autoclave's innermost cylinder and heats both the air within the autoclave as well as the rest of the autoclave's insulation and structural elements. The material properties used for the air and the autoclave's structural components are defined in Table 3.

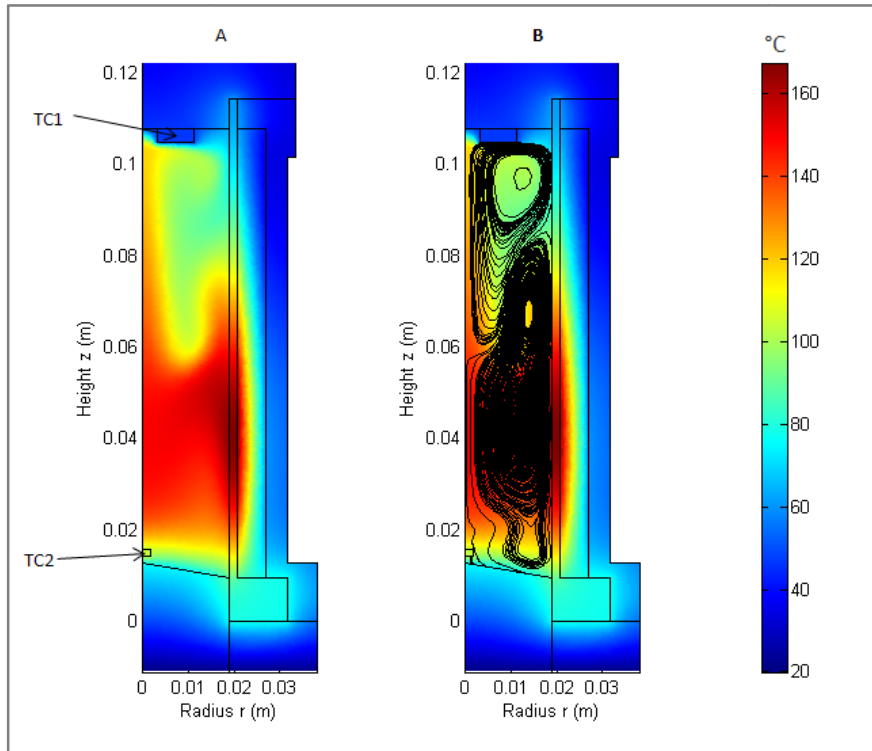


Figure 5: Model 0A at t = 500 seconds

Natural convection and conduction dominate the heat transfer and fluid flow within the air, and conduction dominates through the autoclave's structural solid materials. Accordingly EQ. 17 was applied so the autoclave's structural subdomains, and EQ. 18, EQ. 21, and EQ. 22 were solved within the fluid air region. At the interfaces between the air and the autoclave structure, boundary conditions BC 2 and BC 6 were applied. At the external (atmosphere) boundary condition BC 4 was applied. For the heater location at the interface between the insulation and stainless steel autoclave walls BC 5 was applied, and for all other structural interfaces BC 1 was applied.

Once the model had been run, the transient temperature profile at two points (Figure 5 A), TC 1 and TC2, within the autoclave were obtained. To validate the model against

experimental data, thermocouples were placed into the actual MiDA autoclave at the same two locations, and an autoclave cycle identical to the one just described was run. The temperature profile for the modeled data was then compared with the temperature profile measured by the thermocouples to assess the accuracy of the modeling techniques.

Case 1: Dry Sample

Case 1 included all model scenarios in which a dry sample is introduced to the bottom of the autoclave chamber and no water is added from the water reservoir.

Model 1A

For the first model representative of a plausible MiDA sterilization scenario, the sample bulk was located at the bottom of the chamber (Figure 6C). The sample volume was 25mL, and it was assumed to enter the chamber dry. No water was added from the water reservoir, and there was no sample contamination on the inner walls of the chamber. The sample distribution was wide (sample contacts the walls), and it is assumed that there were no large air pockets anywhere within the sample bulk. This meant that the sample bulk was of uniform density, and the top layer of sample was assumed to be flat. The material properties of the sample bulk were defined by Table 3 assuming a porous media composed of quartz sand and air.

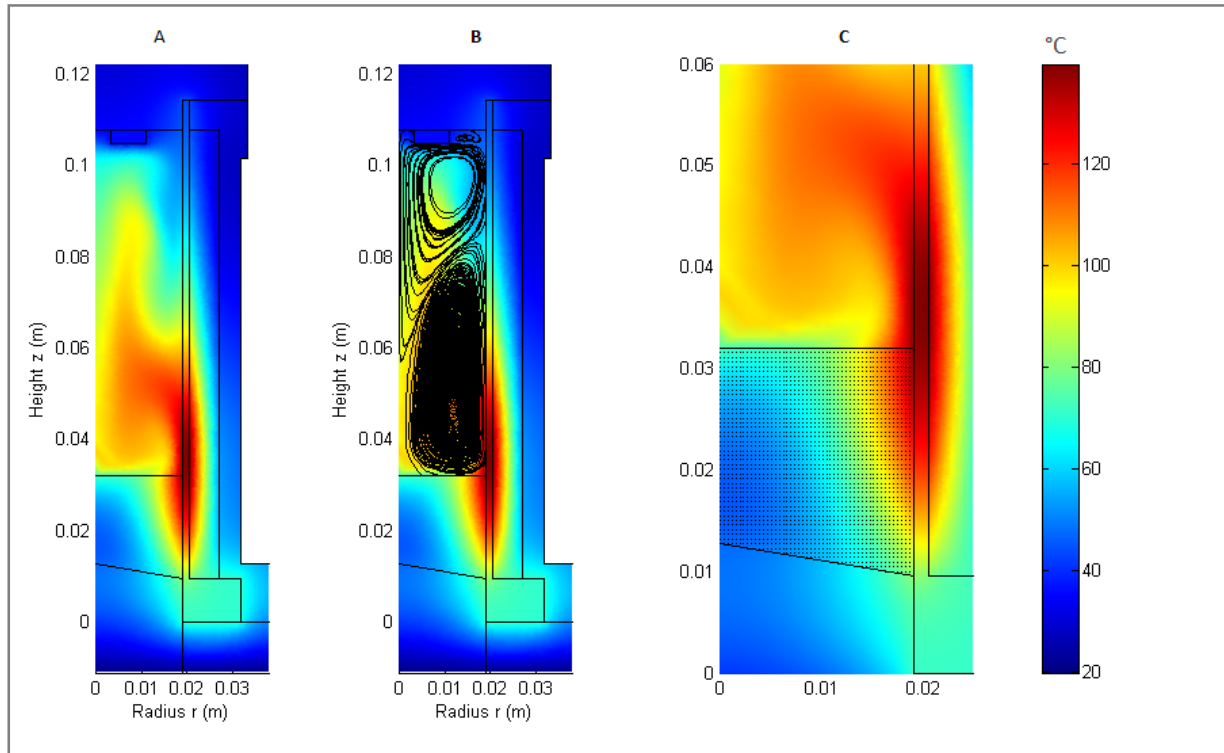


Figure 6: Model 1A at t = 500 seconds

Once the autoclave heaters are turned on, heat is transferred through the stainless steel walls of the autoclave's innermost cylinder and heats both the air and sample within the autoclave. Heat is transferred directly into the sample from the air above the sample, from the bottom of the autoclave, and from the autoclave walls. Natural convection and conduction dominate the heat transfer and fluid flow within the air above the sample, and conduction dominates through the autoclave's structural solid materials. Conduction is also assumed to be the only mechanism of heat transfer within the sample bulk.

Accordingly EQ. 17 was applied so the autoclave's structural subdomains, and EQ. 18, EQ. 21, and EQ. 22 were solved within the fluid air region. At the interfaces between the air and the autoclave structure and the air and the sample bulk, boundary conditions BC 2 and BC 6 were applied. At the external (atmosphere) boundary condition BC 4 was applied. For the heater

location at the interface between the insulation and stainless steel autoclave walls BC 5 was applied, and for all other structural interfaces BC 1 was applied.

Since it is unknown where in the sample living organisms would be present, it will be assumed that they were located uniformly through the sample bulk at a regular spacing defined by a 25 by 25 mesh within the sample bulk (Figure 6 C). The model organism was E coli, and it was assumed that the organisms were immobile within the sample bulk and the temperature of a concentration of organisms at each mesh point was equal to temperature of the sample bulk at each mesh point.

Model 1B

Model 1B was identical to model 1A with the adjustment of increasing the sample volume to 50 mL to gauge the effect of varying sample volume on the sterilization process. As can be seen in Figure 7 the sample bulk subdomain was increased appropriately to model a sample bulk size of 50 mL. All equation and boundary condition assignments remained the same as in model 1A.

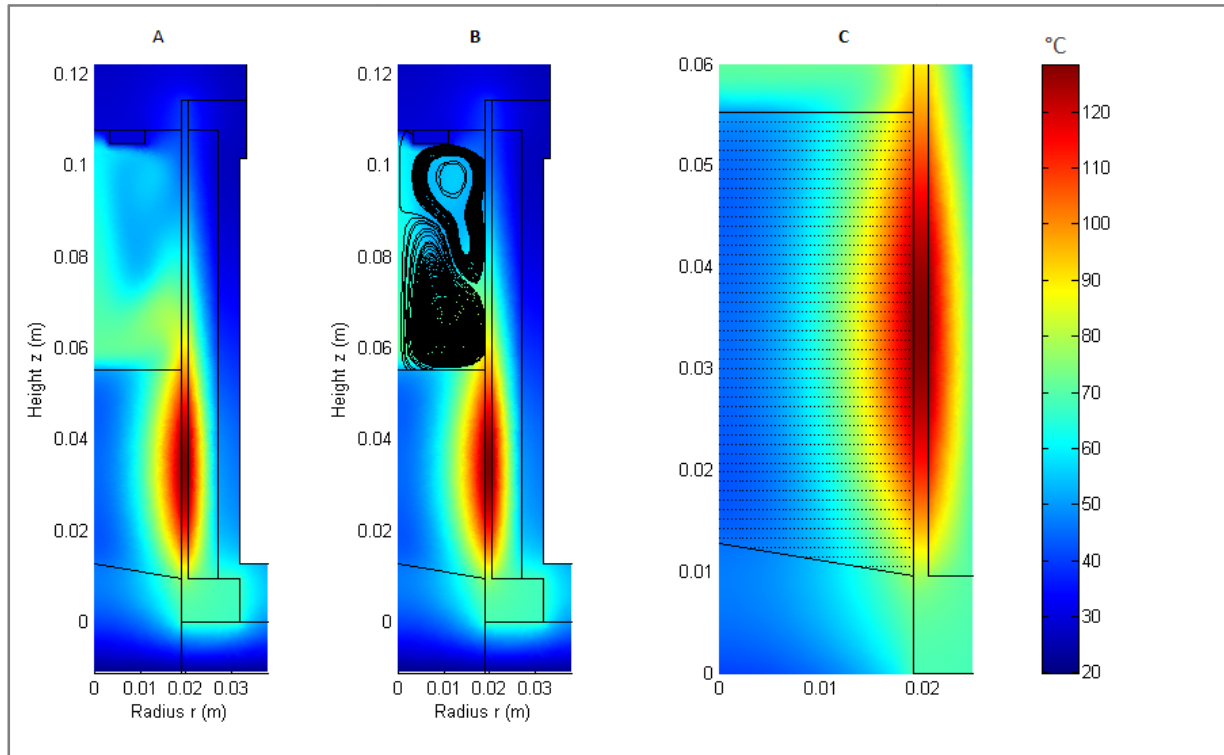


Figure 7: Model 1B at t = 500 seconds

Model 1C

Model 1C studied the sample distribution by assuming a narrow sample distribution of the 25 mL volume from model 1A (Figure 8). Accordingly, heat is transferred through the stainless steel walls of the autoclave's inner walls to only the air and not to the sample bulk this time. In this scenario natural convection and conduction from the hot air dominate the heat flow. This is in contrast to the large heat flux from walls to the sample surface in the case of a wide sample distribution. The only adjustment made for this scenario was in the geometry of the sample subdomain and the application of BC 2 and BC 6 to the surfaces of the sample and autoclave structure now exposed to air.

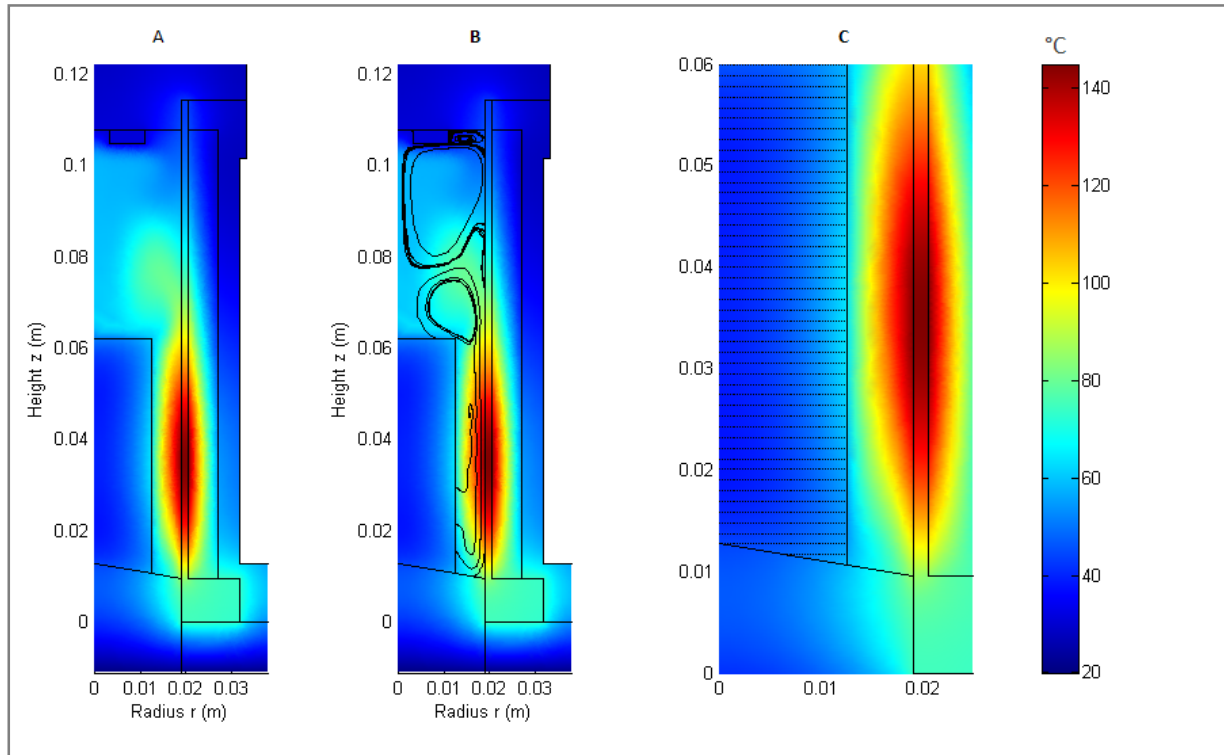


Figure 8: Model 1C at t = 500 seconds

Case 2: Sample and Water Addition

Case 2 included all model scenarios in which a sample is introduced to the bottom of the autoclave chamber and varying amounts of water are added from the water reservoir for use during the autoclaving process.

Model 2A

Model 2A was the same as model 1A with the exception that a “minimal” level of water was added from the water reservoir (Figure 9). This had the effect of simply changing the thermal properties of the sample bulk, and accordingly the sample bulk’s material properties are defined by Table 3 assuming a porous media composed of quartz sand and water.

As with the scenarios for case 1, the model organism is E coli, and it was assumed that the organisms were immobile within the sample sediment and the temperature of a concentration of organisms at each mesh point is equal to temperature of the sediment at each mesh point.

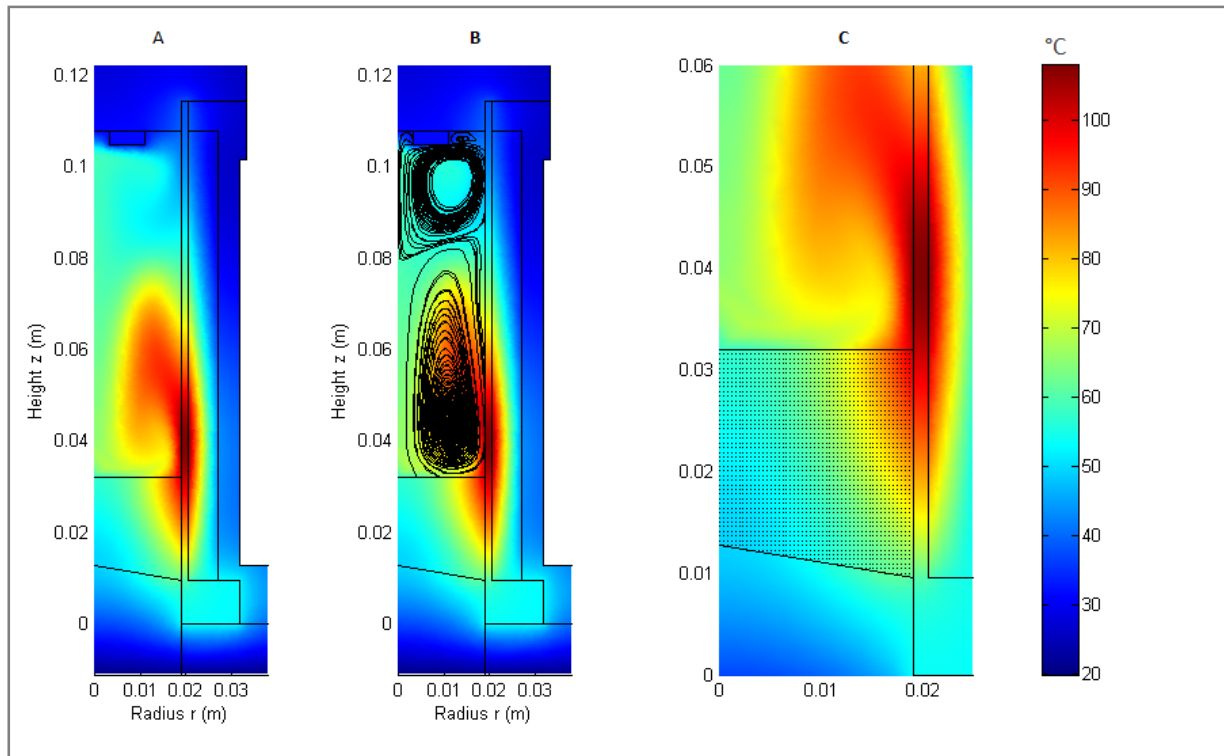


Figure 9: Model 2A at t = 500 seconds

Model 2B

Model 2B is similar to model 2A with the exception that an excess level of water was added to a bulk sample of 25 mL. The amount of water was 25mL plus enough to completely replace air as the matrix for the sample bulk, and accordingly, this model included a water subdomain of 25mL above the sample (Figure 10). It was assumed that the sample remained as sediment at the bottom of the chamber during the process. The important realization for this model is that now there are two fluid phases, air, and liquid water. Heat transfers from the walls

of the chamber to both fluid phases (as well as the sample bulk) and their thermal profiles are influenced by both conduction and natural convection. The sample water phases exchange heat and so do the two fluid phases.

As before, heat transfer through the autoclave structure and sample bulk sediment is characterized purely by conduction, and accordingly EQ. 17 was applied to those subdomains. Convection and conduction characterizes the heat transfer through both the liquid water and air phases. For the compressible gas phase and equations EQ. 18, EQ. 21, and EQ. 22 were applied to the appropriate subdomains, and EQ. 18, EQ. 19, and EQ. 20, were applied to the incompressible liquid phase.

For the new boundary conditions at the air fluid interface, BC 7 was applied on the fluid side, and BC 8 was applied on the gas side. All other boundary conditions were the same as previously stated.

For this model, as opposed to model 2C, it was assumed that no organisms enter the fluid phase and that they remain evenly distributed in the sample sediment, similar to model 2A.

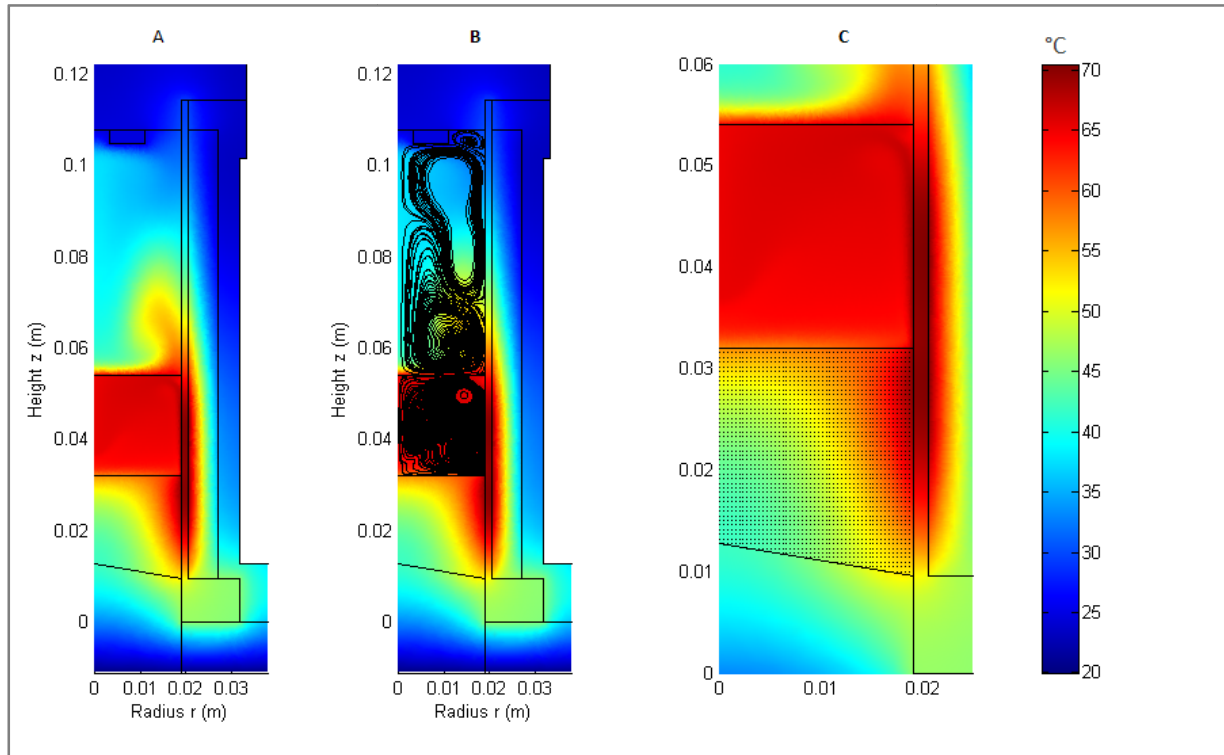


Figure 10: Model 2B at $t = 500$ seconds

Model 2C

This model was similar to model 2A with the exception that the adhesion of the organisms to the sample were such that it allowed them to enter the liquid water fluid phase above the sample bulk and be transported with the natural convection (Figure 11). As a limiting case, it was assumed that the entire concentration of the organisms initially present in the sample bulk, became uniformly distributed on a 25 by 25 mesh throughout the fluid phase at time $t=0$. Once natural convection started to occur due to heating, the locations of the organisms were tracked with time by retrieving the induced velocity profile. It was assumed the individual concentrations of organisms, initially at mesh evenly spaced locations, followed the streamlines of the flow exactly, and that there was no slip between the organisms and the fluid. A temperature history for each mesh point (concentration of organisms) was determined by

assuming that the temperature of the organisms continually matched the temperature of the fluid at their mesh location. The temperature profile and the locations of the organisms at $t = 500$ seconds is shown in Figure 11 C. It should be noted that a similar scenario will arise if a sample composed completely of liquid is considered.

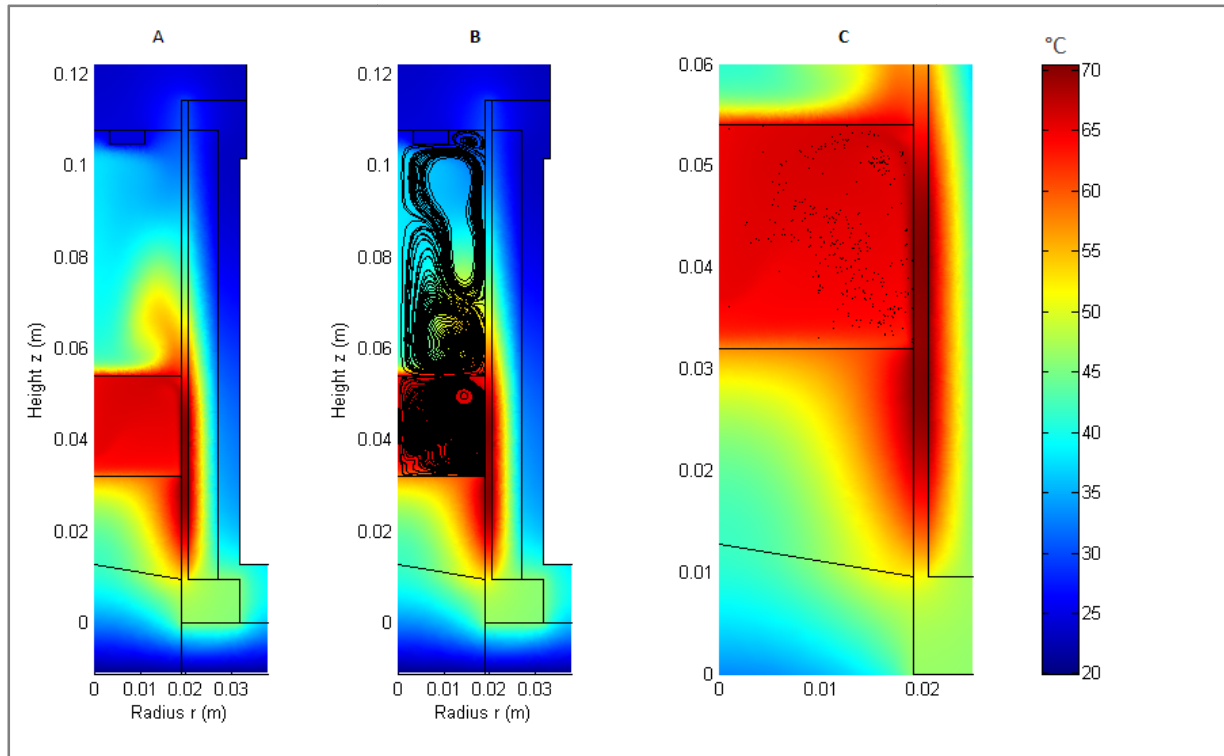


Figure 11: Model 2C at $t = 500$ seconds

Model 2D

Model 2D was the same as model 2B with the exception that the stirrer at the bottom of the autoclave was used to force fluidization of the entire sample bulk and water into a mixture. In this model, the mixing forced the temperature of the mixed slurry to be uniform, and any heat transfer effects to the slurry other than those of convection from the walls could be neglected. Momentum effects between the mixed slurry and air were neglected since they would not affect the temperature profile in the slurry. The uniformity of the sample temperature was

created by modeling the slurry region with a k value of infinity. The other thermal properties were defined by EQ. 16 and assuming that $\epsilon = 0.9$. Any interaction between particles was neglected. The locations of organism concentrations was again modeled by a uniformly spaced 50 by 50 mesh.

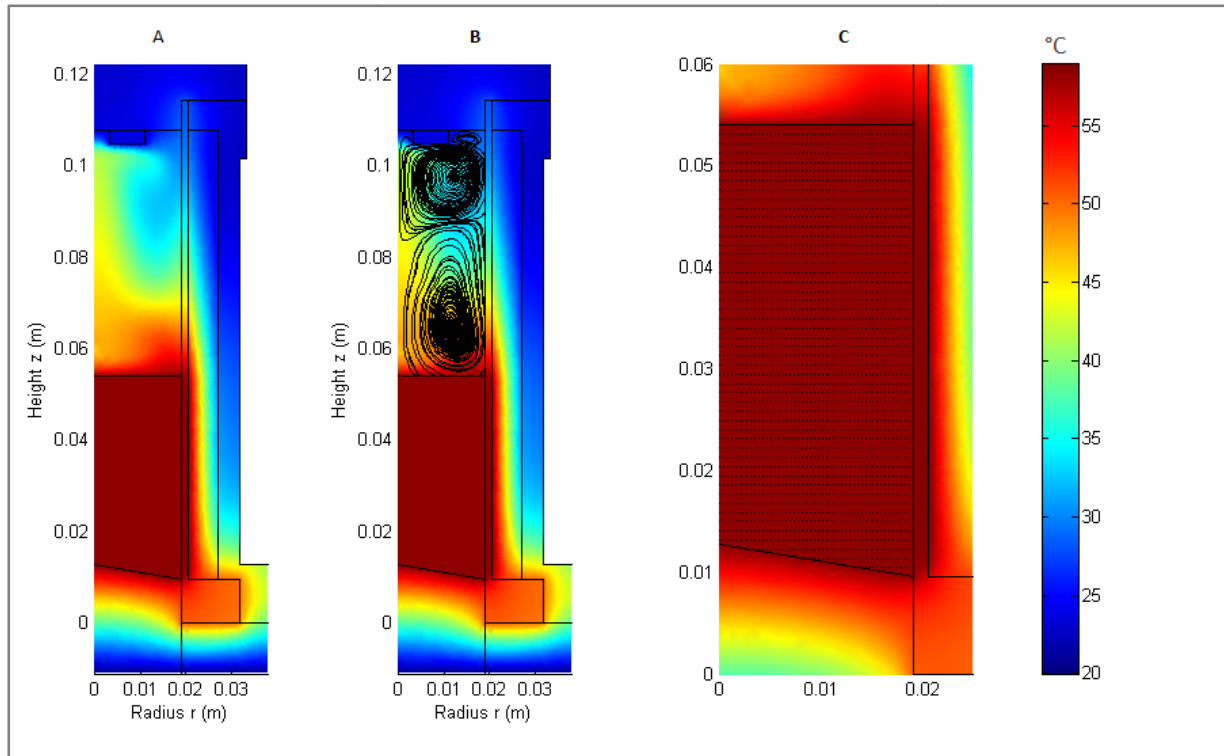


Figure 12: Model 2D at $t = 500$ seconds

Summary

The properties of each of the models described above are summarized in Table 4.

Table 4: Summary of MiDA Model Scenarios

Model	Sample Volume	Sample Distribution	Water Volume	Org. Adhesion to sample	Stir
1A	25 mL	wide	none	N/A	N/A
1B	50 mL	wide	none	N/A	N/A
1C	25 mL	narrow	none	N/A	N/A
2A	25 mL	wide	min. mat.	N/A	N/A
2B	25 mL	wide	excess	sediment	off
2C	25 mL	wide	excess	Fluidized	off
2D	25 mL	wide	Excess	Forced fluidized	on

*For all of the above scenarios the organism choice was E Coli, and the sample material was quartz sand.

A transient temperature profile at each organism mesh location was determined from the results of all the above thermal models. Next, F and Q values were determined throughout time for every mesh point using EQ. 11 and EQ. 12. Accordingly, it was possible to obtain the Q values throughout the sample (at every mesh point) at any point in time. SQDs were generated by first selecting a specific point in time and plotting a histogram of the Q values throughout the sample mesh using a bin size of $Q = 0.5$. The final steps in generating the SQDs was normalizing the histogram by the total number of bin counts and smoothing the results to create the SQD curves. The following sections discuss the SQD results for each MiDA model scenario and assess their implications for MiDA autoclave operation.

Model Validation

Before comparing the SQDs of the MiDA modeling scenarios, it was necessary to assess the results of the model 0A for validation of the modeling procedures against experimental data. As described previously, the temperature profile at two locations within the MiDA autoclave was determined using both the Comsol FEA modeling process and experimentally with measurements taken from thermocouples placed within the real MiDA autoclave. The locations of the thermocouples (TC1 and TC2) and a snapshot of the thermal modeling results at $t = 500$ seconds are shown in Figure 13. Throughout the heating process, it is clear that the temperature measured by the thermocouples shows large consistent temperature gradients between the upper and lower regions of autoclave chamber, ranging by as much as $70\text{ }^{\circ}\text{C}$ (Figure 13C). Figure 13A also shows that the absolute temperatures in the convective flow can range as much as $100\text{ }^{\circ}\text{C}$. A comparison of the temperature profile between experimental data and modeled data at both locations is shown in Figure 13C.

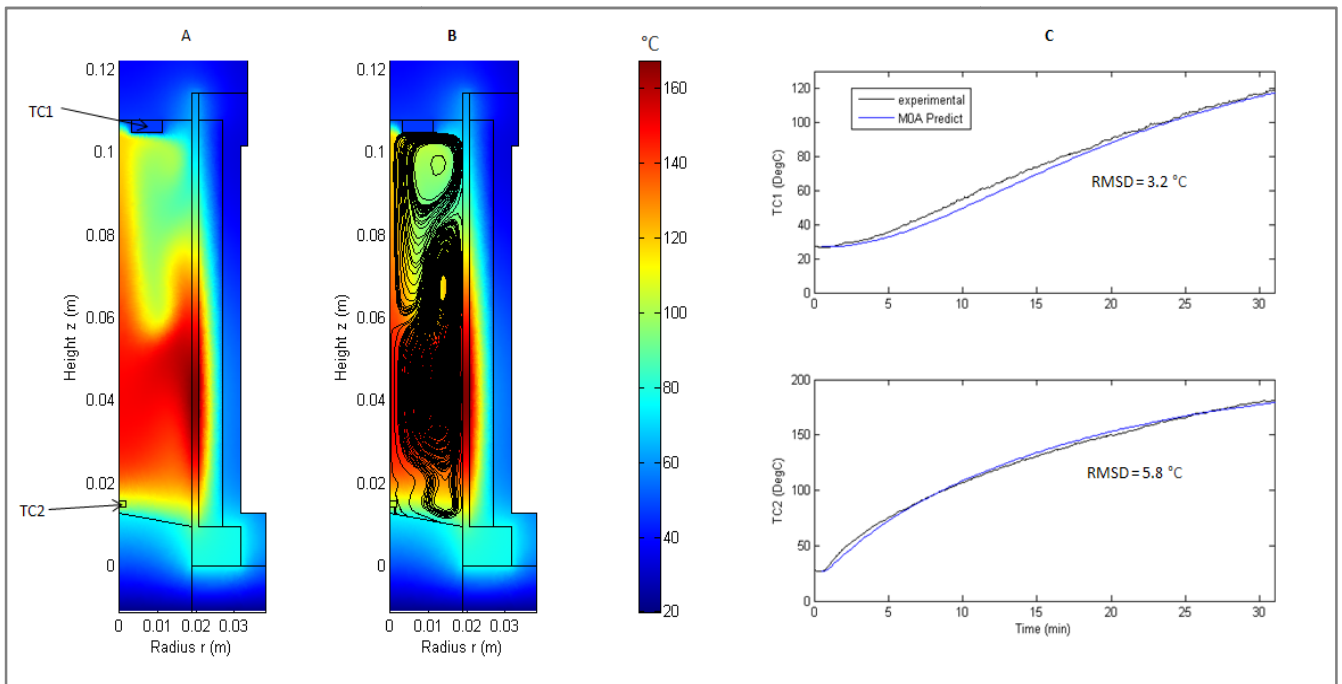


Figure 13: Comparison of Model 0A to experimental data. The temperature profile with the autoclave was measured experimentally with TC1 and TC2 placed at the top and bottom of the autoclave. The profiles obtained from the thermal models at those two locations are in great agreement with the experimental data.

The comparison between temperature recorded from the thermocouples and the temperature data from the thermal models is in great agreement. The agreement in the data is particularly good considering the large temperature gradients. The RMSD values for both curves are no worse than 4% of the range of the signal. The inflections in the curve are modeled well, and it appears that both systems will eventually reach a similar steady state. The agreement of the temperature profile predicted by the model and the experimental data proves that thermal modeling procedure used for predicting the temperature profile within the MiDA autoclave is valid.

Evaluation of a Single Scenario

To begin a comparison of the SQD results between models, it is instructive to first consider the results from just one of the simplest models. Figure 14 shows the SQD for model 1A at an arbitrary time of $t = 300$ seconds. For all of the upcoming analyses Q_{Target} was defined such that it represents a 10 decade decrease in organism concentration.

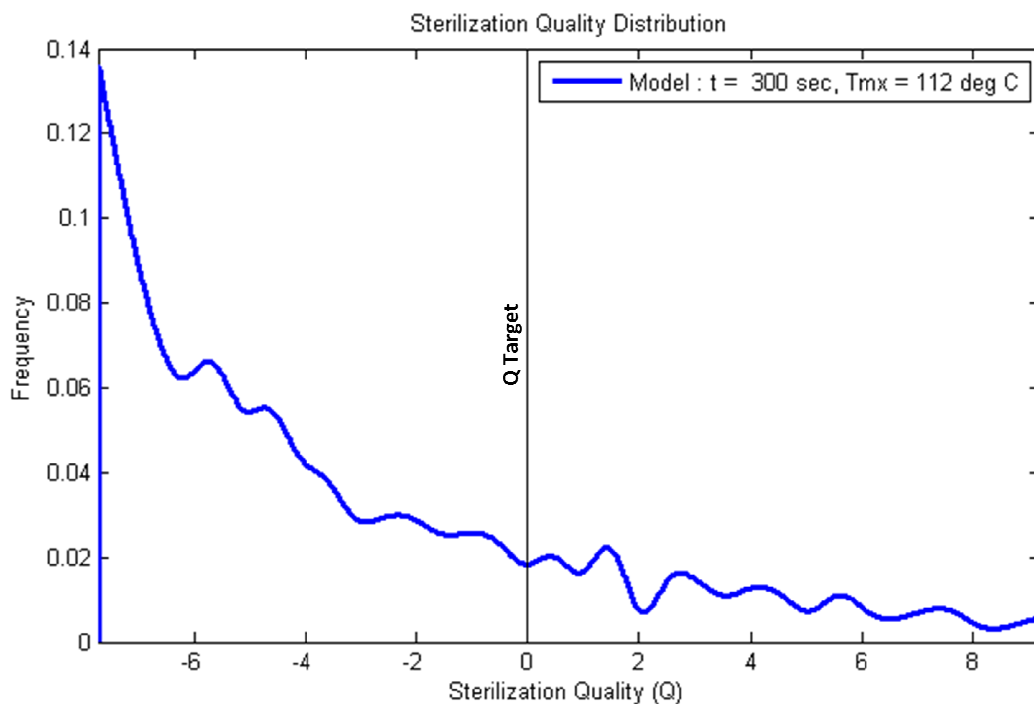


Figure 14: Model 1A SQD at $t = 300$ seconds

Figure 14 shows that at 300 seconds a small portion of the sample has met the target Q value (of $Q = 0$), while there is still a significant amount left to reach it. By summing the frequency data on either side of Q target and dividing by the total sum of the frequencies, the result shows that 21% of the sample has reached the target value while 79% still has not. Qualitatively, the diagram shows that the portion of the sample above $Q = 0$ has experienced high time-temperature effects, while those to the left have seen less. In this specific scenario it is

likely that those points to the right of the peak are likely influenced by the high temperatures from the wall heaters, while the points to the left are more towards the cooler center portion of the sample. The peak frequency value, occurring at the minimum Q value of around -7, indicates that there is still a large portion of the sample that is still well below lethal temperatures for E Coli. It is also instructive to observe a plot of how the SQD for model 1A changes throughout time. Such a plot is shown in Figure 15.

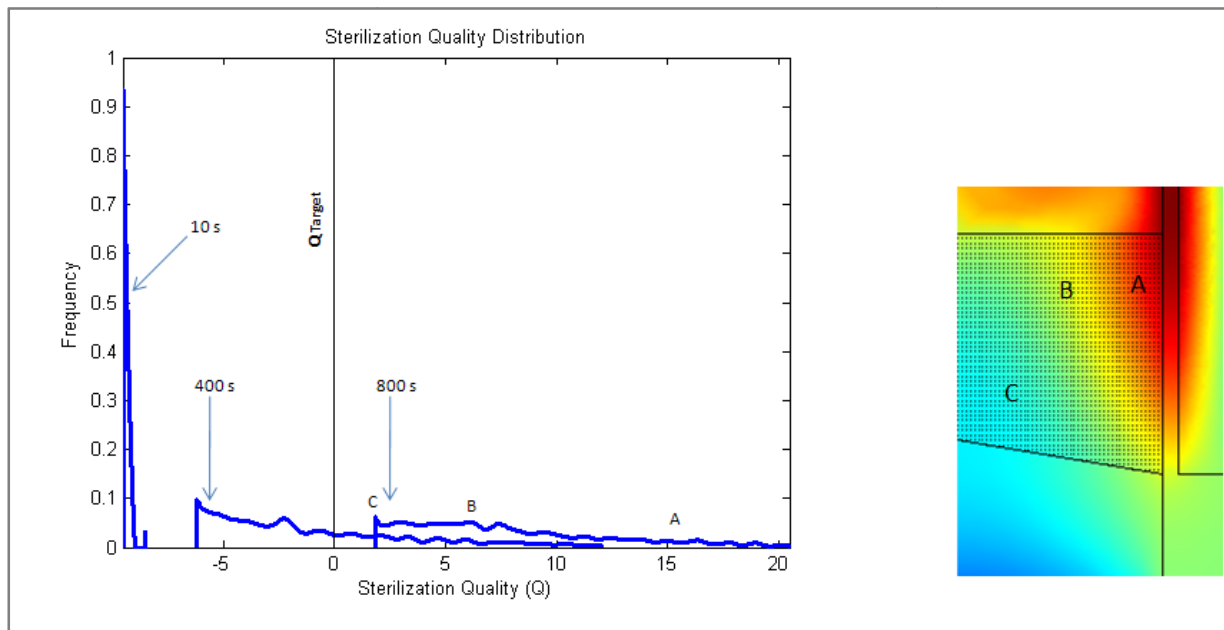


Figure 15: Time series of the SQD for model 1A

It is clear that at times close to $t = 0$, all the points start with similar sterilization quality values, and as time goes on, certain regions sterilize faster and others slower, thus widening the distribution and lowering its maximum height. The shape of the distribution is also often representative of the geometry of the system. For example, the thermal profile of the autoclave

at 800 seconds is shown in Figure 15, and it is likely that the points A, B, and C on the thermal profile, match portions A, B, and C of the SQD at 800 seconds.

One primary use of a single SQD is to be able to determine the length of time it takes to for various percentages of the sample to reach a target sterilization value for a given scenario. For example, it took between 800 and 800 seconds for model 1A to reach the target sterilization value. A single SQD is also useful in determining the result of a particular sterilization process such as determining that at 400s, 35% of the sample had seen at least a 10 decade reduction in organism concentration. Several other uses of SQDs become apparent when plotting the SQDs of several different scenarios together on the same axes.

Time Limit SQD Comparison

The first method of comparing SQDs was performed by plotting the SQDs for multiple processes at the same point in time. The resulting plot gives useful information for situations when the total time of the sterilization process is of concern for media degradation. In such situations, it will often be the case that the best process to choose is the one that reaches a high quality of sterilization the quickest. For example, comparing MiDA scenarios 1A-C and 2A-D at a time limit of 700 seconds results in the SQDs shown in Figure 16.

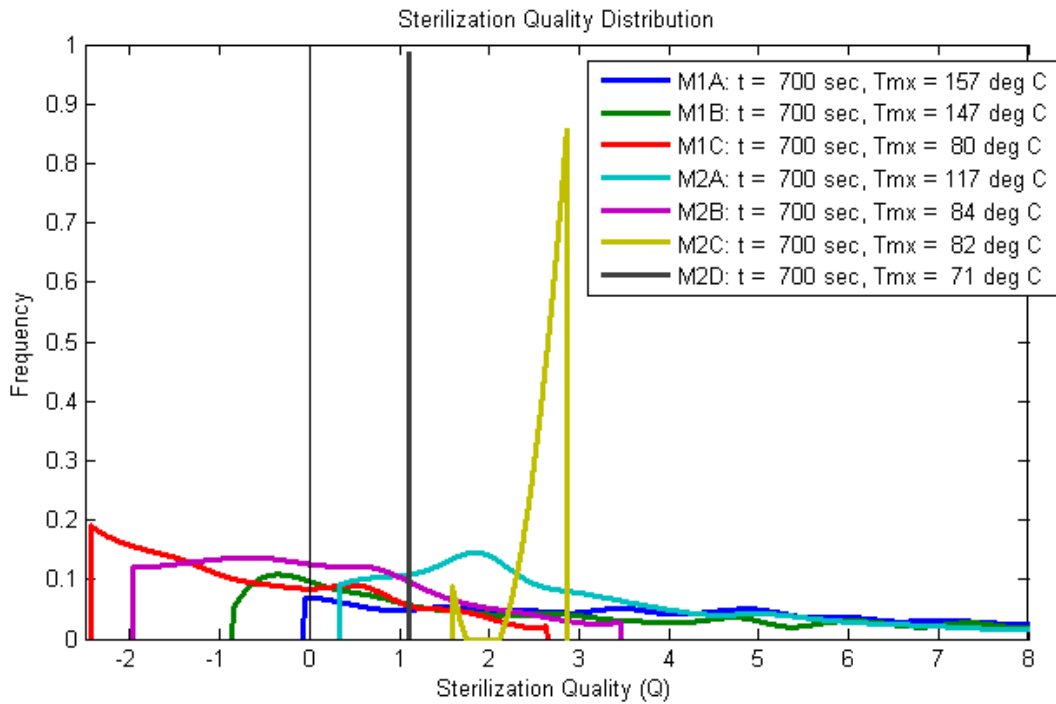


Figure 16: Sterilization quality distributions of MiDA model scenarios limited by $t = 700$ seconds

Qualitatively, Figure 16 easily shows that the scenario M2C is the quickest to reach full sterilization followed by M2D, M2A, and M1A. It is also worthwhile to realize that the distributions of M1A and M1B are extremely wide compared to the other scenarios, likely due to the low thermal conductivity of the sample bulk and larger sample volume (for M1B) creating large thermal gradients. This is in contrast to model 2D in which stirring creates a uniform temperature throughout the sample bulk, resulting in a very narrow distribution. Quantitative results from these SQDs are summarized in Table 5.

Table 5: Results from SQD limit of 700 seconds

Model	SQD Time (s)	T_{mx} (°C)	Sample Above Q_{Target} (%)	WSQ⁴
1A	700	157	99	5.8
1B	700	147	84	4.5
1C	700	80	33	-0.6
2A	700	117	100	3.2
2B	700	84	50	0.1
2C	700	82	100	2.6
2D	700	71	100	1.1

From the results in Table 5 and by observing Figure 16, it is clear that models 2C and 2B, and 2D are the best to use if a time near 700 seconds is desired for sample preservation. It is valuable to note that for a process like 2B, qualitative observations and quantitative results complement each other especially well. Even though the WSQ of model 1A of 5.8 indicates it may have reached the target sterilization quality, an observation of Figure 16 clearly shows a small portion has not. However, the observation also reveals that scenario 1A may be worthwhile to run if it is possible to run for just slightly longer. It is also interesting to note that, while scenario 2B has a WSQ above the target value, it still has one of the lowest minimum Q values, and 50% of the sample is still below the target sterilization quality. This highlights the need to base decisions on both the numerical results and qualitative observations from the SQD curves. It is also important to realize that the maximum temperature reached within the sample for each of the SQDs varies by up to 86 °C at this point in time, and if high temperatures are of concern to media degradation a separate method of comparison is needed to determine what process is best.

⁴ The weighted sum of Q (WSQ) is the sum of the product of Q*frequency for a SQD curve.

Temperature Limit SQD Comparison

If a particular temperature limit is of concern for media degradation, it is useful to compare the SQDs at the times when any portion of the sample bulk first reaches that temperature limit. For the analysis here, an example temperature limit of 100 °C was used. Figure 17 shows SQDs for MiDA models 1A-C and 2A-D plotted at the moment in time when any location within the sample bulk first reaches 100 °C.

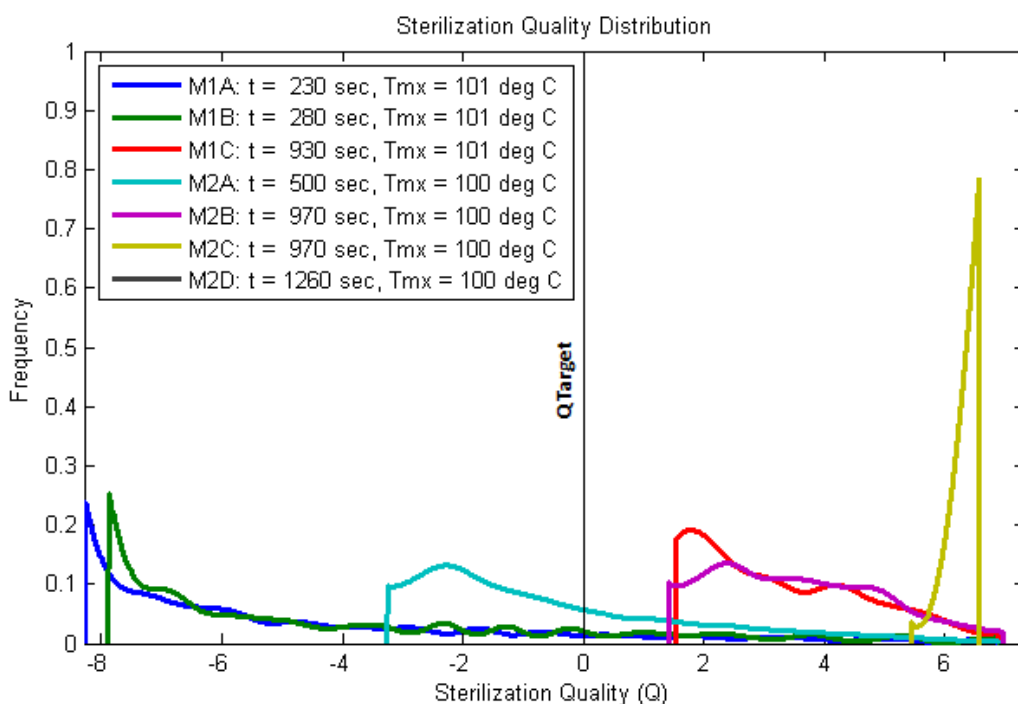


Figure 17: Sterilization quality distributions of MiDA model scenarios limited by $T_{mx} = 100\text{ }^{\circ}\text{C}$

A qualitative interpretation of the SQDs shows that M2D best achieves full sterilization while avoiding high temperature, followed by M2C, M2B, and M1C. The SQD diagram aids in selecting processes that have the ability to run to full sterilization without reaching a prescribed

temperature limit, thus preserving the samples chemical properties while achieving full sterilization.

Table 6: Quantitative results for a $T_{mx} = 100\text{ }^{\circ}\text{C}$ comparison

Model	SQD Time (s)	T_{mx} ($^{\circ}\text{C}$)	Sample Above Q_{Target} (%)	WSQ
1A	230	100	14	-4.5
1B	280	100	18	-3.9
1C	930	100	100	3.4
2A	500	100	34	-0.4
2B	970	100	100	3.6
2C	970	100	100	6.2
2D	1260	100	100	7.3

The quantitative results show that the WSQ values of scenarios 1C, 2B, 2C, and 2D indicate values above Q target and suggest they are good candidates for achieving Q target while keeping the temperature below $100\text{ }^{\circ}\text{C}$.

Again, the quantitative and qualitative results complement each other well. Even though models 2A has a WSQ value close to $Q = 0$, an observation of SQD diagram shows that a dangerously large portion of it is actually still below $Q = 0$.

If the properties of a sample are unknown, it may not be particularly useful to strictly apply either of the two previous comparison methods. Instead, a method is needed to gauge both temperature and time effects simultaneously.

Time-Temperature Comparison

A comparison of models in terms of both time and temperature effects can be achieved by comparing SQDs plotted at the moment in time when all points within the sample bulk have reached a certain minimum target Q value. Such a plot for MiDA scenarios 1A-1C and 2A-2D is shown in Figure 18, and the quantitative results are in Table 7. The limiting Q value is the target of $Q = 0$.

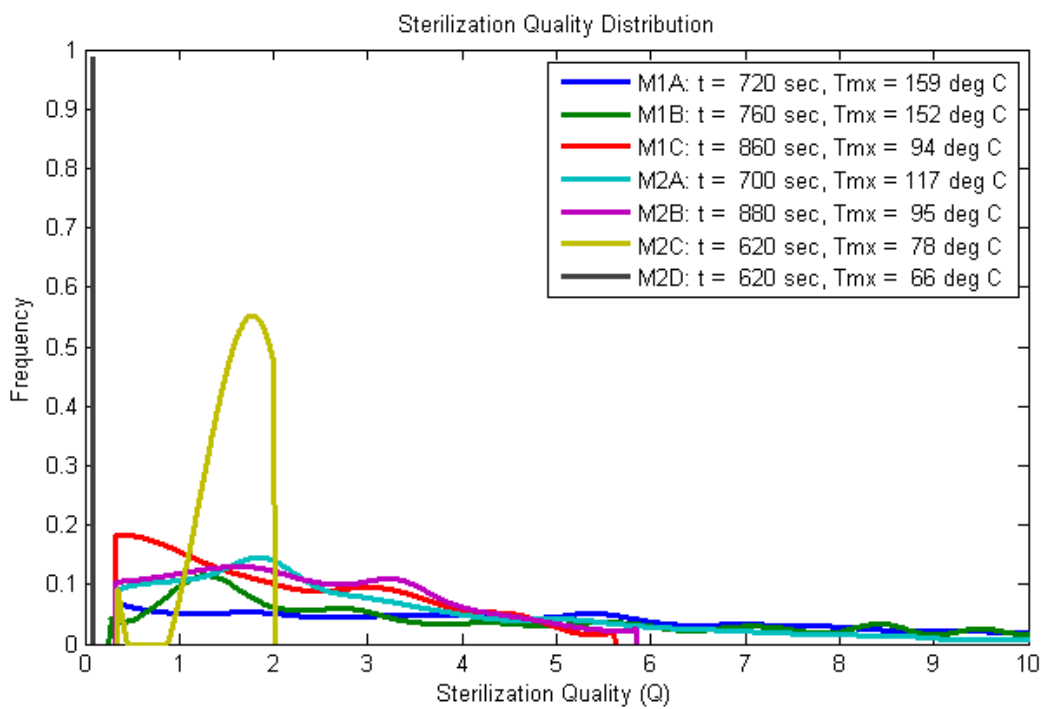


Figure 18: Sterilization quality distributions of MiDA model scenarios limited by $Q_{min} = 0$ (10D reduction)

Table 7: Quantitative results for a $Q_{min} = 0$ comparison

Model	SQD Time (s)	T_{mx} (°C)	Sample Above Q_{Target} (%)	WSQ
1A	720	159	100	6.2
1B	760	152	100	5.7
1C	860	94	100	2.1
2A	700	117	100	3.2
2B	880	95	100	2.5
2C	620	78	100	1.6
2D	620	66	100	0.1

As stated in the beginning of the methodology section, a plot that is limited by Q indicates that points farther to the right have generally received higher cumulative time-temperature effects than those to the left. Thus, SQDs for which the majority of points have lower Q values will have seen cumulative time-temperature effects. This indicates that scenarios with narrow distributions along Q, such as M2D, M2C, and possibly M1C are generally the best in achieving low cumulative time-temperature effects. Accordingly those three models also have the lowest Q values of 0.1, 1.6, and 2.1 respectively. This result makes sense since 2D has the lowest temperature and takes the least amount of time to reach the full sterilization requirement. This is a very useful result if it is unknown what may degrade in the sample due to temperature and time, and a general optimization of those parameters is desired without any specific time or temperature constraints. On the other hand, if media degradation is simply not a concern, one should simply go with the scenarios that give the highest WSQ values. On the SQD diagram, that corresponds to scenarios 1A and 1B with WSQ values of 6.2 and 5.7 respectively.

Comparison Between Organisms

By plotting the SQDs for the case in which *Bacillus subtilis* is the organism being sterilized, it was found that there were slight changes in the order of preference for the scenarios due to the longer durations and higher temperatures required to sterilize *Bacillus Subtilis* (Table 8). The decimal reduction time and z-value of *Bacillus subtilis* are 11 minutes and 100 °C respectively, as opposed to 2.5 min 58 ° C for *E. coli*.

Table 8: Comparison of results for E coli and B Subtilis

Model	Sample Above Q_{Target} (%)	E. Coli SQD Time (min)	B. Subtilis SQD Time (min)	E. Coli T_{mx} (°C)	B. Subtilis T_{mx} (°C)
1A	100	12	22	159	200
1B	100	13	24	152	195
1C	100	14	26	94	148
2A	100	12	22	117	157
2B	100	15	45	95	130
2C	100	10	26	78	131
2D	100	10	24	66	109

Comparison between Sample Properties

It was also worthwhile to determine whether the sample material properties had a significant influence on the overall sterilization process. Accordingly, two additional variations on model 1A were run with the sample particles composed of the minerals hematite and pyrite instead of quartz. The thermal properties of hematite and pyrite compared to quartz are shown in

Table 9. A SQD plot of the two additional scenarios, along with M1A, is show in Figure 19. They are plotted at the time when they each reach $Q=0$

Table 9: Thermal Properties of Samples of Quartz, Hematite, and Pyrite

Material	k (W/m·K)	ρ (kg/m ³)	Cp (J/kg·K)
Quartz	3	2620	830
Hematite	12	5260	654
Pyrite	23	4900	520
Sample Quartz/Air	0.12	918	944
Sample Hematite/Air	0.12	1841	882
Sample Pyrite/Air	0.12	1716	835

*All mineral thermal conductivity parameters determined from [35]. All mineral Cp and ρ data from [38].

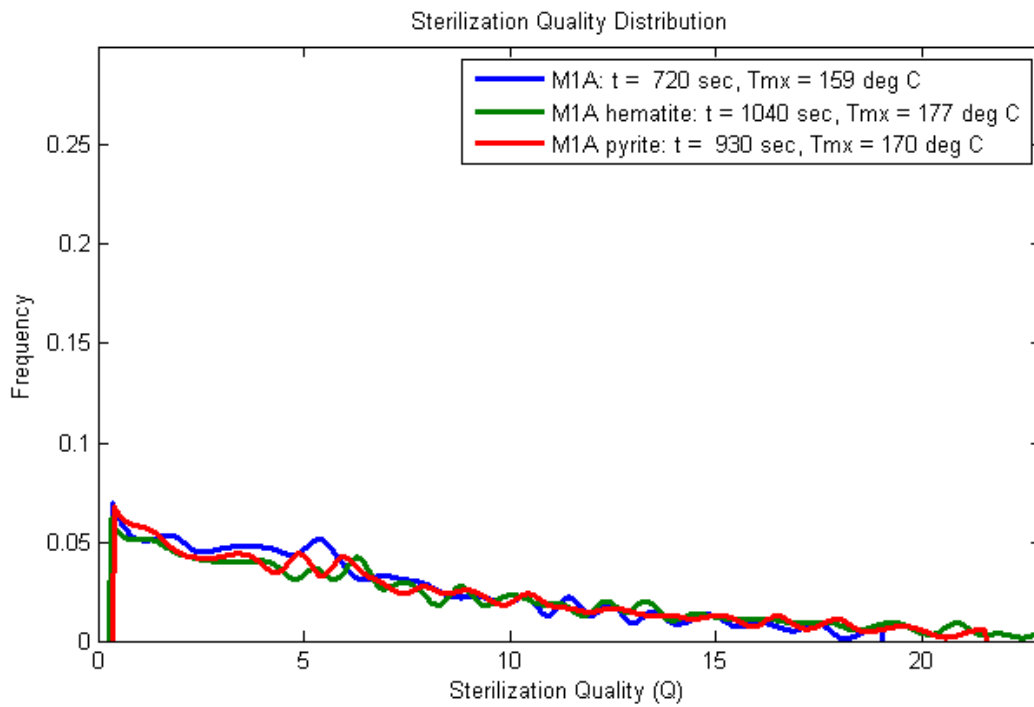


Figure 19: SQDs comparing sample bulk composed of particles of quartz, hematite, and pyrite.

Figure 19 indicates that there are minimal differences in the SQD results when any of these three minerals are considered for the sample bulk. The differences in the temperatures required for full sterilization were around 20°C, and the total times for full sterilization differed by less than 4 min. These small differences are likely due to the similarity in the thermal

conductivities of the sample bulk, which are influenced much more heavily by the air matrix than by the sample particulate material (as predicted by EQ. 15). Thus, the small time and temperature differences arise due to the smaller variations in density and heat capacity between samples.

Conclusions

Assessment of SQD Method

From the discussions in the results section is clear that the SQD method is very useful in both qualitatively and quantitatively comparing how well a wide variety of sterilization processes can achieve sample sterilization with minimal media degradation. Plotting SQDs with time as a limiting factor helped assess which sterilization processes will proceed the quickest. Plotting SQDs with temperature as a limiting factor helped determine which processes can achieve sterilization at the lowest temperatures, and plotting SQDs with a minimum sterilization limit will help minimize both time and temperature effects. The results also indicate that it is necessary to use both quantitative and qualitative methods of analysis to make full use of the SQD curves. These conclusions indicate that the SQD method will be useful in deciding between operational scenarios when using the MiDA autoclave in proof-of-concept studies, and they also may help aid in making future design adjustments. Similar conclusions apply if optimization of both temperature and time effects is required.

Recommendations for Autoclave Operation Under Various Constraints

There are several conclusions that can be reached from the discussion of the results that have implications for the way MiDA will be run in proof-of-concept studies. To begin, if time is of concern for sample degradation, it is best again to run the sample as wet as possible and to use the stirrer if applicable. Next, if temperature is of concern, it is first best to run the sample with the addition of excess water and to stir the mixture during the sterilization process. However, if

the sample cannot be wet, then it is best to run a dry sample while preventing it from contacting the hot walls of the chamber.

Lastly, if sample degradation is not of concern, M1A and M1B have the highest WSQ values on an SQD plot limited by $Q=0$, and this indicates that a dry sample will achieve the best quality of sterilization. However, if the sample cannot be run dry, the next best scenario is M2A, which also indicates that if water is needed, it is best to use as little as possible if the highest sterilization quality is the only requirement.

In general it will take between 10 and 15 minutes for an organism like E coli to reach full sterilization, and it is possible to sterilize E coli at temperatures as low as around 65 °C in that amount of time. On the other hand, for Bacillus subtilis, full sterilization takes between 20 and 45 minutes, and it is difficult to do so below 100 °C. Thus, if media degradation above 100 °C is of concern, organisms more like E coli may be preferred for proof-of-concept studies.

Future Work

For simplicity in the modeling process, only the heating phase of the sterilization process was considered in this work. It is suggested that future work on this subject include considerations of the cooling phase as well since the temperatures at the initial portion of the cooling phase will still be high enough to contribute to the sterilization quality. The sample may continue to degrade during that time as well. Furthermore, MiDA has the capability to perform basic on/off thermal control to adjust or hold the temperature of the autoclave during the sterilization process. Such capabilities should be taken into account to determine whether more efficient thermal profiles than just a simple ramp are possible.

Also, sterilization experiments should be performed in the MiDA autoclave with standard autoclave bioindicators such as *Bacillus Stearothermophilus* to experimentally validate the results generated in this work. Next, an important realization of applying the results of this work, is that it is necessary to characterize the sample media and organisms that will be used in MiDA experiments. This includes knowing DRT and z-values of the organisms used in testing, and temperature and time, limits for media degradation. Lastly, it would be worthwhile to implement some lessons learned from this analysis into the MiDA design. For instance, when high temperatures are of concern and a sample needs to remain dry, it may be worthwhile to install a mesh “basket” that will hold the sample and protect it contacting the hot walls of the autoclave.

Appendices

Appendix A: Effect of Calculations for Thermal Conductivity

To test the effect of different methods for calculating the thermal conductivity for porous media, three equations were applied to Model 1A. These equations included, Hadley's weighted average, the Maxwell Lower Bound, and the Maxwell Upper Bound. The thermal conductivities for the sample bulk (quartz/air) for those three predictions were 0.08, 0.12, and 0.81 W/m·K respectively. The Maxwell bounds serve to define upper and lower limits to the thermal conductivity of a porous media composed of particulates embedded within a matrix such as air or water, and the Hadley Weighted Average serves as an intermediate between the two that tends to agree better with experimental data. A SQD plot of the three scenarios plotted at the time when they reach $Q=0$ is shown in Figure 20.

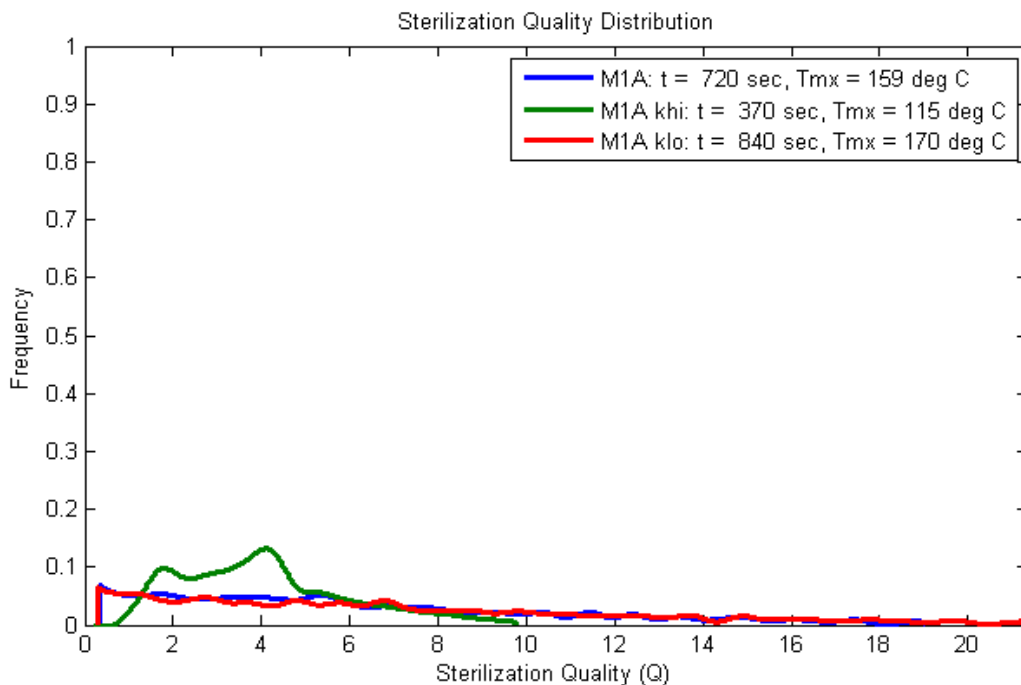


Figure 20: SQD plot comparing methods for calculating thermal conductivity.

The differences in total time and highest temperature vary widely between each of these models. The Maxwell upper and lower bound equations differ by more than a factor of two in total time, and they differ by 55°C in temperature. The Hadley Weighted Average tends to correlate better with the data from the Maxwell Lower Bound. The significant discrepancies between the three predictions indicate that experimental data may be necessary to accurately model the thermal conductivity for specific samples of interest.

Appendix B: Effect of Mesh Size

To test the effect of mesh size on the final SQDs, several different mesh sizes were applied to Model 1A. The original mesh size used was a 25x25 mesh, and the test included mesh sizes of 10x10 and 50x50.

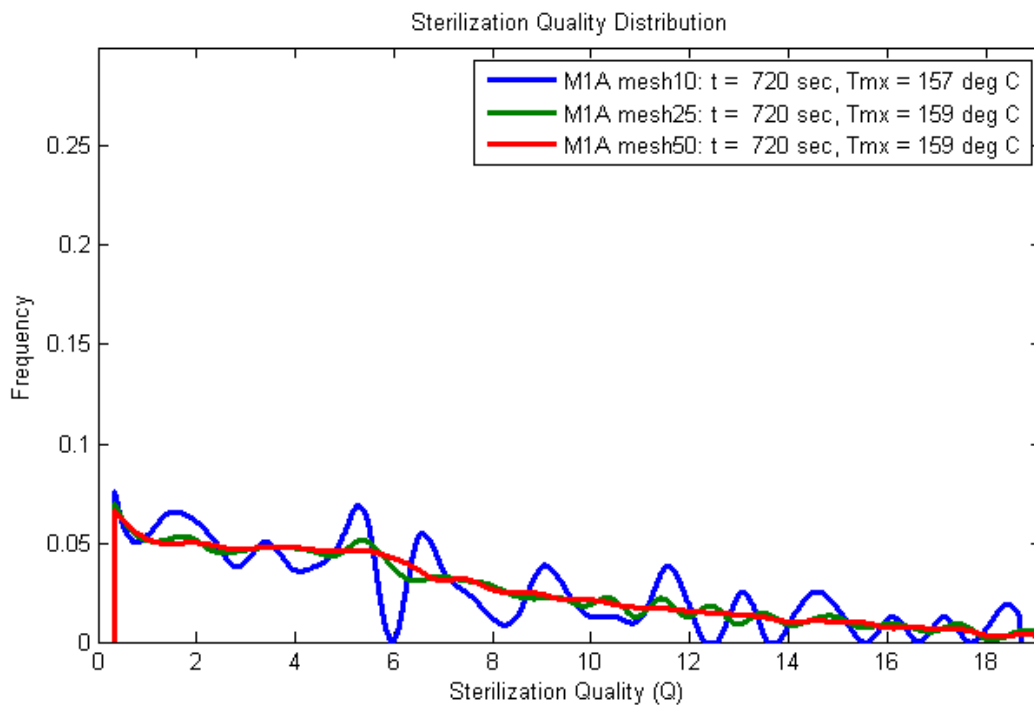


Figure 21: Effect of mesh size on SQD results

As seen in Figure 21, the mesh size has almost no noticeable effect on total time or highest temperature predictions for the sterilization models. The only difference found was that higher resolution meshes generate smoother SQDs. This effect is due to the higher resolution meshes having smaller differences in temperature between neighboring mesh points.

References

- [1] Navarro-Gonzalez, et al. “Mars-Like Soils in the Atacama Desert, Chile, and the Dry Limit of Microbial Life”. *Science*. **302** (2003) 1018 – 1021.
- [2] Hecht, et al. “Detection of Perchlorate and the Soluble Chemistry of Martian Soil: Findings from the Phoenix Mars Lander”. *Science*. **325** (2009) 64-67.
- [3] Mancinelli. “PROSPECTS FOR THE EVOLUTION OF LIFE ON MARS: VIKING 20 YEARS LATER”. *Adv. Space Res.* **22** (1991) 471-477.
- [4] Klein et al. *The Viking Biological Investigation: Preliminary Results*. *Science*. **194** (1976) 99-105.
- [5] Levin and Straat. *A search for a nonbiological explanation of the Viking Labeled Release life detection experiment*. *Icarus*. **45** (1981) 494-516.
- [6] Squyres. “In Situ Evidence for an Ancient Aqueous Environment at Meridiani Planum, Mars”. *Science*. **306** (2004) 1709 – 1714.
- [7] Rothschild. “Earth Analogs for Martian Life. Microbes in Evaporites, a New Model System for Life on Mars”. *Icarus*. **88** (1990) 246-260.
- [8] Nicholson et al. *Resistance of Bacillus Endospores to Extreme Terrestrial and Extraterrestrial Environments*. *Microbiology and Molecular Biology Reviews*. **64** (2000) 548–572.
- [9] Benton C. Clark. *Temperature–time issues in bioburden control for planetary protection*. *Advances in Space Research*. **34** (2004) 2314–2319.
- [10] Boston, Ivanov, and McKay. “On the Possibility of Chemosynthetic Ecosystems in Subsurface Habitats on Mars”. *Icarus*. **95** (1992) 300-308.
- [11] Baker. “Water and the Martian Landscape”. *Nature*. **412** (2001) 228-236.
- [12] Jakosky and Phillips. “Mars’s Volatile Climate History”. *Nature*. **412** (2001) 237-244.
- [13] Nicholson. “Using Thermal Inactivation Kinetics to Calculate the Probability of Extreme Spore Longevity: Implications for Paleomicrobiology and Lithopanspermia”. *Origins of Life and Evolution of the Biosphere*. **33** (2003) 621–631.
- [14] Jakosky. “Subfreezing Activity of Microorganisms and the Potential Habitability of Mars’ Polar Regions”. *Astrobiology*. **3** (2003) 343-350.

- [15] Kounaves, et al. "The MECA Wet Chemistry Laboratory on the 2007 Phoenix Mars Scout Lander". *J. Geophys. Res.* **114** (2009) E00A19.
- [16] Kounaves, et al. "Detection of Microbial Life in Soil Based on Minimal Assumptions Using Measurements of Physical and Chemical Changes Induced by Growth." Seventh International Conference on Mars, California Institute of Technology, Pasadena, CA, July 2007, Abstract No. 3328.
- [17] Klein, et al. "The Viking Biological Investigation: Preliminary Results". *Science*. **194** (1976) 99-105.
- [18] Ponnampereuma, et al. Possible Surface Reactions on Mars: Implications for Viking Biology Results. *Science*. **197** (1977) 455-457.
- [19] Levin and Straat. "A Search for a Nonbiological Explanation of the Viking Labeled Release Life Detection Experiment". *Icarus*. **45** (1981) 494-516.
- [20] Stoforos. "Thermal process design". *Food Control*. **6** (1995) 81-94.
- [21] Ball, C. Olin. *Sterilization in food technology; theory, practice, and calculations*. McGraw-Hill. New York, 1957.
- [22] McKee and Gould. A simple Mathematical Model of the Thermal Death of Microorganisms. *Bulletin of Mathematical Biology*. **50** (1988) 493-501.
- [23] Lee and Singh. Determination of Lethality and Processing Time in a Continuous Sterilization System Containing Particulates. *Journal of Food Engineering*. **11** (1990) 67-92.
- [24] Fellows. *Food Processing Technology*. Woodhead Publishing. Cambridge, 2000.
- [25] Montville and Matthews. *Food Microbiology: An Introduction*. ASM Press. Washington, D.C., 2005.
- [26] Teixeira, et al. Computer Simulation of Variable Retort Control and Container Geometry as a Possible Means of Improving Thiamine Retention in Thermally Processed Foods. *Journal of Food Science*. **40** (1975) 656-659.
- [27] Teixeira, et al. "Computer Optimization of Nutrient Retention in the Thermal Processing of Conduction-Heated Foods". *Food Technology*. **23** (1969) 845-850.
- [28] Silva et al. "Optimal Sterilization Temperatures for Conduction Heating Foods Considering Finite Surface Heat Transfer Coefficients". *Journal of Food Science*. **57** (1992) 743-748.
- [29] Saguy and Karel. Optimal Retort Temperature Profile in Optimizing Thiamin Retention in Conduction-Type Heating of Canned Goods. *Journal of Food Science*. **44** (1979) 1485-1490.

- [30] Ohlsson. Optimal Sterilization Temperatures For Sensory Quality in Cylindrical Containers. *Journal of Food Science*. **44** (1980) 1517-1521.
- [31] Bhowmik and Tandon. A Method for Thermal Process Evaluation of Conduction Heated Foods in Retortable Pouches. *Journal of Food Science*. **52** (1987) 202-209.
- [32] Kaviany. *Principles of Heat Transfer in Porous Media*. Springer. New York, 1995.
- [33] Nepomnyashchy, Velarde, and Colinet. *Interfacial Phenomena and Convection*. Chapman and Hall. New York, 2000.
- [34] Jalali and Li. An estimate of random close packing density in monodisperse hard spheres. *J Chem-Phys*. **120** (2004) 1138-1139.
- [35] Clauser and Huenges. Thermal Conductivity of Rocks and Minerals. *Rock Physics and Phase Relations: A Handbook of Physical Constants*. AGU, 1995.
- [36] Bhuiyan and Koch. Thermal decomposition of struvite and its phase transition. *Chemosphere*. **70** (2008). 1347–1356.
- [37] Kwok et al. Effect of Thermal Processing on Available Lysine, Thiamine and Riboflavin Content in Soymilk. *J Sci Food Agric*. **77** (1998) 473-478.
- [38] Robie and Hemmingway. Thermodynamic Properties of Minerals and Related Substances at 298.15 K and 1 Bar (10^5 Pascals) Pressure and at Higher Temperatures. *U.S. Geological Survey Bulletin 2131*. United States Printing Office. Washington, 1995.
- [39] *Building and Solving a Natural Convection Model-Laminar Flow*. Comsol Multiphysics Documentation. 2008.
- [40] *Modeling Guide*. Comsol Multiphysics Documentation. 2007.